NTNU – Trondheim
Norwegian University of
Science and Technology

Control of Grid Connected Active Converter

Design of Control Strategies for Grid
Synchronization

Han Wee Low

ABSTRACT

Application of power electronics in power distributed generation industry has been a fast evolving technology. This is due to the rapid shift from conventional non-renewable energy source to renewable energy source which led to the rapid rise of distributed generation. Efficient power generation from renewable energy source is highly dependant of the efficiency of the power electronics converter. Thus control of power electronics converter has been a vastly researched subject.

In this thesis, a conventional cascaded control structure serves as a model for grid synchronization control design. Current and voltage control design and simulation will be the main research focus. Control system strategies are divided into approach with different type of controllers, hysteresis and proportional integral controller. It is further subdivided into approach with different control signal reference frame which consist of three phase stationary abc reference frame, two phase stationary $\alpha\beta$ and synchronous dq reference frame. On top of this, a new voltage control structure approach which sees independent control of voltage magnitude and voltage frequency-phase angle is implemented too.

In order to verify the theoretical study, simulation model is built and run for each methodologies presented. Control with PI controller in synchronous dq frame is found to be more reliable despite the pros and cons of each approach. Further detailed results and discussion of various applications together with proposal for future research are presented in the end of the thesis.

ACKNOWLEDGEMENT

First and foremost, I would like to thank Professor Lars Einar Norum, my supervisor in Norwegian University of Science and Technology (NTNU) for his experienced guidance from the stage of choosing a topic for thesis project till the delivery of the report. He has always been welcoming and supportive for his students and that meant so much to us especially as an international student in NTNU.

I would like to express my greatest gratitude to my external supervisor Professor Roy Nilsen from Wärtsilä, Norway. He has been a great mentor for this thesis project that can be traced back to the summer internship placement. His availability for discussion and his expert guidance has been important in driving this thesis. Moreover this thesis can't be performed without the Simulink converter model at the courtesy of Wärtsilä.

Big thanks to my fellow colleagues in the class of M.sc Electric Power Engineering and energy conversion group in NTNU. All the helps and sharing of problem during this entire project are deeply appreciated.

Last but not least, I would like to thank my beloved family and friends for the support and motivation especially to my girlfriend Jiarui Pang for being extremely supportive and understanding during my long working hours for this project.

ABBREVIATIONS

AC	Alternate current
BW	Bandwidth
CG	Centralised generation
CCL	Current control loop
DC	Direct current
DG	Distributed generation
ERR	Error
GM	Gain margin
IEC	International Electrotechnical Commission
IEEE	Institute of Electrical and Electronics Engineers
MO	Modulus Optimum
NTNU	Norwegian University of Science and Technology
PCL	Power control loop
PI	Proportional integral
PLL	Phase lock loop
PM	Phase margin
PR	Proportional resonance
PV	Photovoltaic
PWM	Pulse width modulator
RMS	Root mean square
SO	Symmetrical optimum
VCL	Voltage control loop

NOMENCLATURE

C_b	filter base capacitance
C_f	filter capacitance
$C(s)$	converter transfer function
f_n	nominal frequency
f_c	cross over frequency
f_{cf}	filter capacitor voltage frequency
f_g	grid voltage frequency
f_{sw}	switching frequency
$G_c(s)$	current control system transfer function
$G_v(s)$	voltage control system transfer function
$G_{OL}(s)$	open loop transfer function
$G_{CL}(s)$	closed loop transfer function
$I_{a,b,c}$	a, b and c - phase current
$I_{d,q}$	d and q-axis current
$I_{\alpha,\beta}$	α and β-axis current
I_b	base current
I_f	converter side filter current
I_g	grid side filter current
I_n	rated current
I_{ref}	reference current
K_p	PI controller gain
K_s	system gain
$L_c(s)$	current control filter system transfer function
$L_v(s)$	voltage control filter system transfer function
L_b	base filter inductance
L_f	converter side filter inductance
L_g	grid side filter inductance
$P(s)$	PI controller transfer function
$P_c(s)$	current PI controller transfer function
$P_v(s)$	voltage PI controller transfer function
R_f	converter side filter resistance
R_g	grid side filter resistance
T_{A-}	converter positive switch
T_{A-}	converter negative switch
T_i	PI controller time constant
T_{sw}	converter switching period
T_α	converter time delay
T_f	filter time constant
$V_{a,b,c}$	a, b and c - phase voltage

$V_{d,q}$	d and q-axis voltage
$V_{\alpha,\beta}$	α and β-axis voltage
V_b	base voltage
V_c	filter capacitor voltage
V_{dc}	converter dc voltage
V_e	converter voltage
V_g	grid voltage
V_n	rated voltage
V_{ref}	reference voltage
Z_b	base impedance
ζ	damping factor
ω_b	base angular frequency
ω_s	synchronous frequency
ω_o	natural oscillation frequency
θ	phase angle for PLL
θ_c	phase angle difference between grid and filter capacitor voltage

CONTENTS

LIST OF FIGURES

LIST OF TABLES

1   INTRODUCTION

This thesis work focus on the current and voltage control strategies for grid synchronization implemented in a cascaded control structure of grid connected converter. The system structure of grid connected active converter and the different methodologies of current and voltage control used in industry have been researched and documented. A Simulink converter model is used for simulation and modelling of the sub systems is developed and presented. There are two types of controller chosen to be implemented in this thesis namely hysteresis controller and proportional integral controller. While these controllers will work in three different reference control frame, stationary *abc* frame, stationary *αβ* frame and synchronous *dq* frame. The results are presented with focus on discussion of differences between the various control strategies. Possible research work for future are proposed in the end of this thesis.

The introduction chapter begins with presentation of the background of electric power generation system and how it leads to the emergence of microgrid concept which provides higher reliability and security in electricity power supply. It will also discuss the technical challenge that lies on the control of active converter which is vital for the robustness of microgrid. This chapter ends with the presentation of thesis objectives and thesis outline.

1.1   BACKGROUND AND MOTIVATION

Traditional centralized generation (CG) is a large scale power generation plant usually located far away from end consumer with heavy reliance on non-renewable resources such as gas, coal and nuclear boiler, although hydro power is used to some extent. Electricity is transmitted and distributed through a large interconnected grid network before reaching end consumer. Environmental impact due to use of non-renewable resources and huge amount of power loss or low efficiency results from long distance of transmission are among the obvious disadvantages of CG. However reliability of the electricity supply is more of a concern especially in the era of massive application of sophisticated electronic devices where consumer loads are critical and sensitive to power disturbance couple with the aging infrastructure of decades old power grid network. In 1996 for example a damaged power line in Oregon left 12 million customers in eight states without electricity [1].

Distributed generation (DG) is an approach to generate electrical power on a smaller scale and located at distribution network as can be seen in Figure 1.1 which is close to consumer load and not stretched across a long transmission network. The growing technology in power generation based on renewable energy sources especially wind and solar power combine with commitment in Kyoto Protocol have led to constant growth of DG [4]. Though at this moment DG may be more expensive on a cost per kilowatt basis [5] but the environment friendly and high efficiency makes DG expected to become more important in the future generation system. Further readings of CG and DG can be found in [2], [3], [9], [11].

Microgrid is simply a smaller version of the large electric grids builds to serve the local electricity needs [6]. It consists of power generation, storage, distribution lines and interconnection to the large network grid via a point of common coupling as shown in

Figure 1.2. The concept arises from the needs for rural electrification but with the integration into large network grid, it has increased the security and reliability of electricity supply. During main grid network supply disturbance, the power generation and corresponding loads in microgrid can isolate from the main grid system. This isolation is usually called islanding. After the separation loads in microgrid will continue to receive power supply from its own power generation plant or energy storage and therefore maintain the electricity supply in microgrid [7]. The advancement of converter's control allows two directional power flow between microgrid and macrogrid [8], and independent control of active and reactive power to meet the dynamic needs of the load.

Meeting local demand and enhancement in grid reliability are the top benefits of microgrids according to research by Zpryme in November 2012 sponsored by IEEE Smart Grid [6]. The reports also assessed that development of microgrids will increase with global capacity of 10 gigawatts to 15 gigawatts on average over the next five years, especially in critical loads such as hospital, military and government facilities. It concluded that over the next five years microgrid can prove to be a viable solution to meet the primary energy needs for industries that are not able to tolerate lost of electricity supply for even a few minutes.

1.2   CHALLENGES AND CURRENT RESEARCH

Integration of microgrid with large network grid or sometimes also known as macrogrid does promise higher security and reliability in electricity supply in general. However there are technical constraints that may degrade the network overall reliability by adding internal failures. Without proper control and regulation in place, failure can be catastrophic where a disruption or blackout of the microgrid is expected. Among the potential adverse impacts commonly discussed include [2], [8], [9]:

- Voltage and current transients during intentional connection and disconnection of microgrid or unintentional disconnection due to sudden lost of grid power.
- Increased of power quality disturbances beyond the level of acceptance for other customers especially in harmonic distortion.
- Inadequacy or incorrect setting of the protection system which could be unexpected operation leading to power supply disruption.

In such an integrated system, the robustness of power electronics converter is of utmost importance. The fast growing and ubiquitous application has pushed the limit of the current technology and thus inspired many research and development in this particular area [10]. The future of power generation lies in the concept of smart grid. It is basically an electrical grid that uses computer based remote control and automation [12]. The implementation will see big improvements in energy efficiency and integrating renewable resources with end consumer to participate in the electricity enterprise. Nevertheless, according to United States Department of Energy, power electronics play a critical role in transforming the current electric grid into the next generation grid [13]. This describes the broad horizon for the need in research and development of power electronics converter. Advance readings for smart grid can be found in [14], [15], [16], [17], [18].
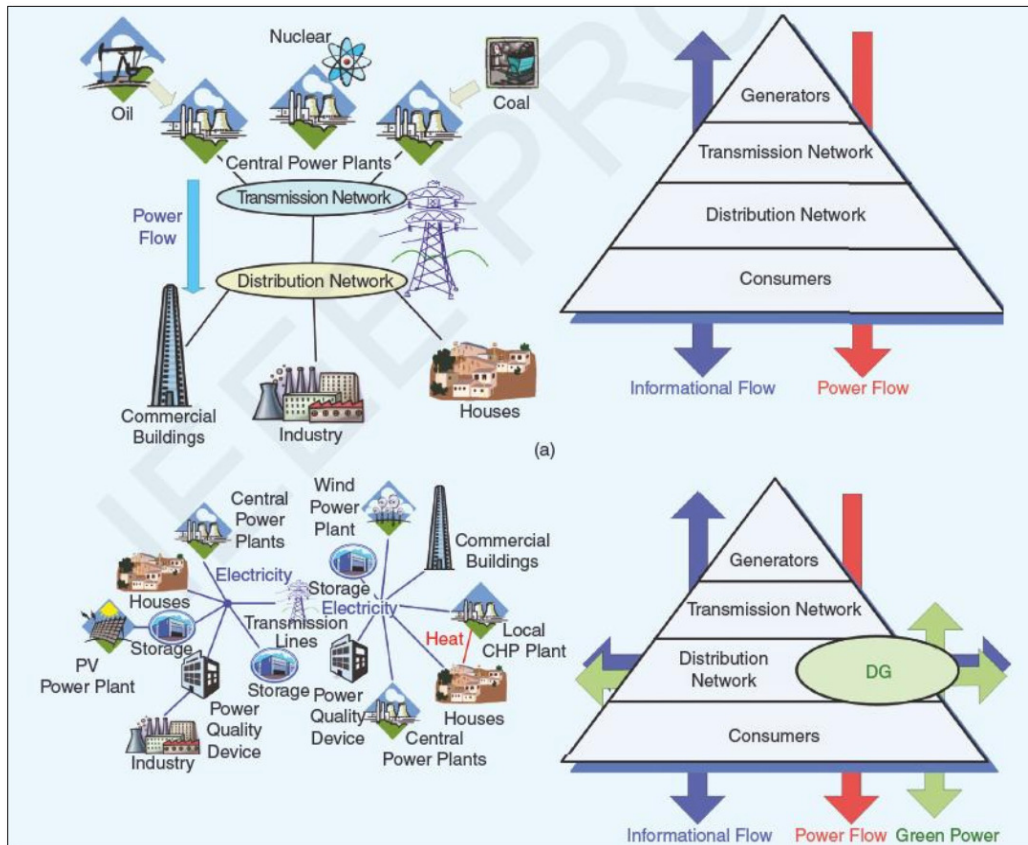
Figure 1.1: Centralised generation and distributed generation system structure [19]
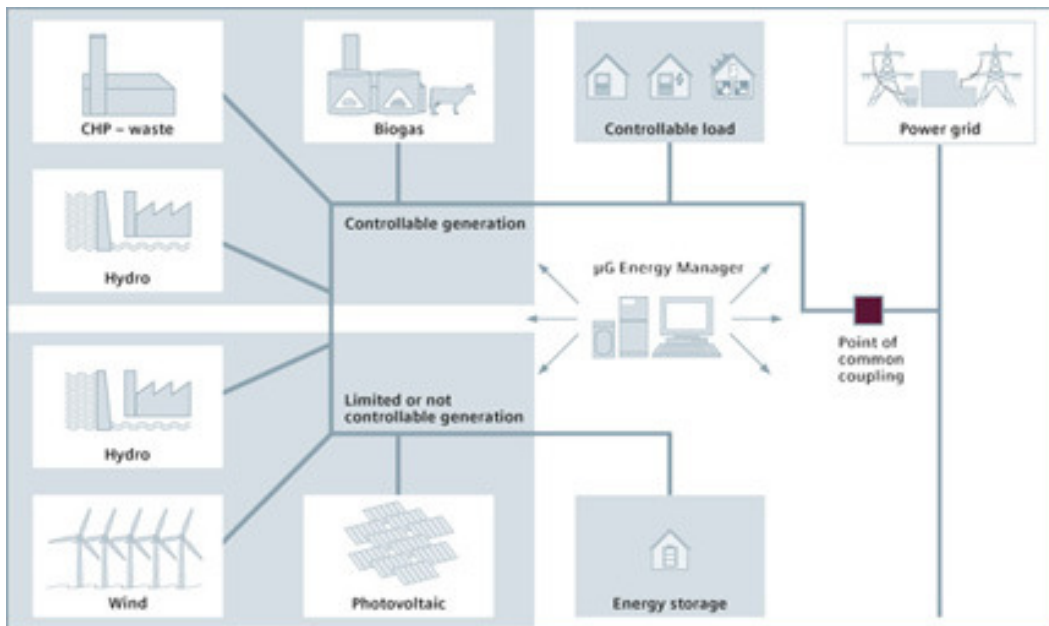
Figure 1.2: Microgrid system structure [20]

1.3 OBJECTIVES OF THESIS

- To investigate cascaded control structure for grid connected converter control which consist of inner current control loop and outer voltage control loop.
- To design a robust current controller and voltage controller with different control strategy
- To compare and discuss each of the different control strategies implemented
- To identify potential improvement and strategy for future research work

1.4 OUTLINE OF THESIS

Chapter 1 gives a brief background introduction on the rise of importance of power electronics application in power grid network industry. The fast growing distributed generation influenced by the growth of renewable energy has pushed for a demanding technology solution for grid connected power converter in terms of its control and capacity. This is one of the main driving factors that initiate global research in relevant topics. The main objectives of this thesis are listed at the end of this chapter.

Chapter 2 reviewed the main grid connection standards that are followed by the industry which is important for the research design to be complied with. This chapter also gives an overview of the grid connected converter structure with its main control function before having more focused overview on control structure and grid LCL filter which are the important elements in this thesis.

Chapter 3 presents the converter control system components and theories which are necessary for readers and researcher of this thesis to acquire before proceeding further. The main components described are the different controller types of PI controller and hysteresis controller along with the optimization methodologies that is used to design the parameter of PI controller. Modulus optimum and symmetrical optimum are the two optimization approach presented. Control signal reference frames are documented in details together with its conversion methods from three phase *abc* stationary reference frame to two phase stationary $\alpha\beta$ reference frame and synchronous *dq* reference frame. In the last section, functional description of pulse width modulation and converter are documented with derivation of its time delay and transfer function representation.

Chapter 4 described in details the control system structure and strategy for grid synchronization. The converter control structure implemented in this thesis is a cascaded control structure consists of inner current controller and outer voltage controller. Each of the current and voltage control system has three different approaches which are fun with illustration. In the voltage control system, PI controller with synchronous *dq* reference frame will be the current control strategy used as the common inner current control loop.

The current control strategy utilizes:
- PI controller in stationary $\alpha\beta$ reference frame
- PI controller in synchronous *dq* reference frame
- Hysteresis controller in stationary *abc* reference frame.

While the voltage control strategies consist of:

- PI controller in stationary *αβ* reference frame
- PI controller in synchronous *dq* reference frame
- Magnitude and frequency-phase angle controller

Chapter 5 starts with derivation of the converter modelling with LCL filter. Mathematical modelling is derived in detailed together with feed forward compensation approach for current and voltage controller. With the transfer function representation, optimization method is applied to find the PI controller's parameter. Stability analysis is carried out with the parameter found to observe the dynamic response of the designed system.

Chapter 6 defined all the parameters implemented in the simulation model in the initial section. These include converter system rating, converter per unit system, LCL filter parameters and criteria for grid synchronization. A brief introduction is given on the simulation model and program used. Subsequently, the simulation results for all current and voltage control strategies as described in Chapter 4 are presented and discussed. The main characteristic, pros and cons of each strategy are the main point for discussion.

Chapter 7 concludes the findings of this thesis research mainly based on the simulation results obtained in Chapter 6. Eventually, proposed works for future research for scope within this thesis to improvise findings and out of this thesis for potential strategy to be investigated.

2 OVERVIEW OF GRID CONNECTED ACTIVE CONVERTER SYSTEM

This chapter gives an overview of grid connected active converter system. In order for the system to be accepted globally, it is important to know the common standard used by the industry. The following sections discuss the overall converter structure and the control system structure which will be the main focus of this thesis. In the last section, overview of the various filter topologies which is connected between the converter and load system are presented.

2.1 GRID CONNECTION STANDARDS

Integrating a distributed power system into electric grid network has a list of requirement that need to be met to ensure a safe connection to grid. A research based on the rules and regulations are necessary for the design of an approved grid connected active converter. The standards applied for interconnections between distributed power system and electrical grid varies around the world. Certain nation and region develops their own standards for the local grid utilities and for different voltage level. However, to a certain degree these standards are similar and mainly based on two major international standards from Institute of Electrical and Electronics Engineer (IEEE) and International Electrotechnical Commission (IEC). The main and most vital requirement and limitations can be found in the standards provided by IEEE and IEC.

The most relevant standard that compiled all technical requirement and test for grid connected distributed generation and operation is the

- IEEE1547-2003: Standard for Interconnecting Distributed Resources with Electric Power Systems [21].

While some standards are developed to be specific such as

- IEC61727: Photovoltaic (PV) system – Characteristics of the utility interface
- IEC61400-21: Measurement and Assessment of Power Quality Characteristics of Grid Connected Wind Turbines
- IEEE1547.3-2007: Guide for Monitoring, Information Exchange, and Control of Distributed Resources Interconnected with Electric Power Systems
- IEEE1547.6-2011: Recommended Practice for Interconnecting Distributed Resources with Electric Power Systems Distribution Secondary Networks

2.2 OVERVIEW OF GRID CONNECTED CONVERTER STRUCTURE

Figure 2.1 below shows the general structure for DG power system with different input power sources. Among various power sources available, photovoltaic, fuel cell and wind turbine system are the most implemented. The technology used in the different power sources is not presented here, however it is well documented in [22], [23], [24] and [25].
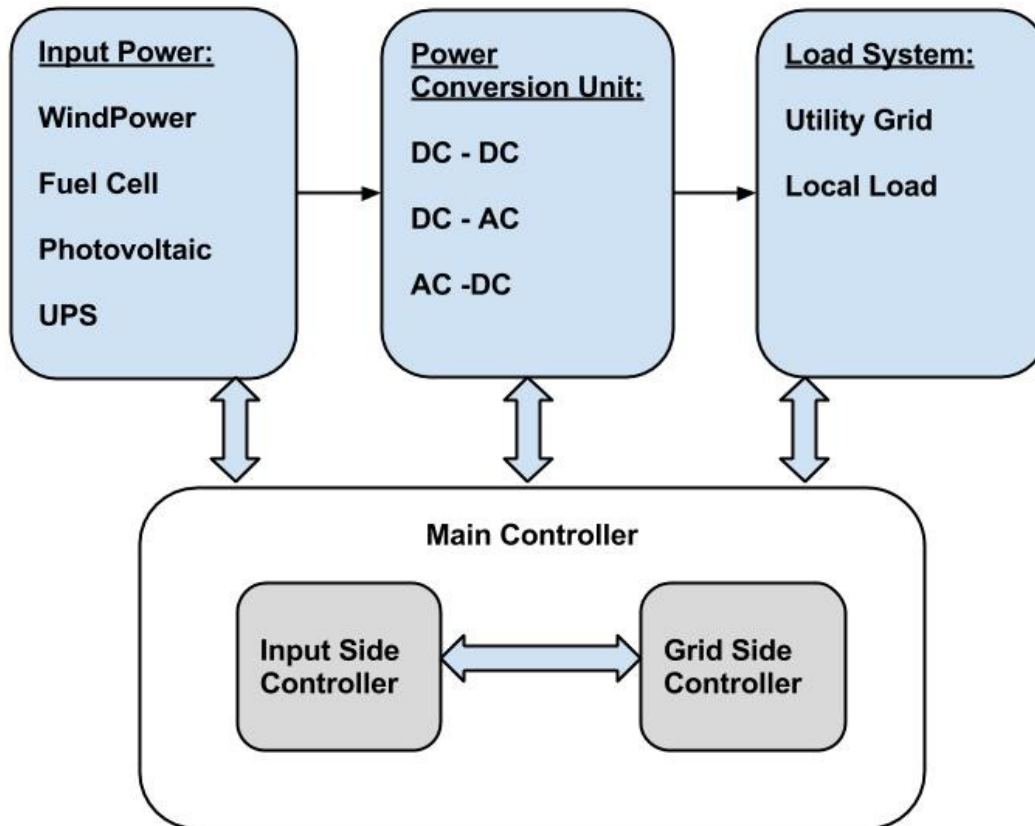
Figure 2.1: General structure for distributed power system with different input power sources [6]

The delivery of electrical power to load system is via a power conversion unit which consist of three basic types, namely (alternate current) AC-DC (direct current), DC-DC and DC-AC. The most essential and critical part in this structure will be the control of power conversion unit as shown in the main controller block in Figure 2.1. The choice of control strategy used for specific configuration will eventually determine the stability and quality of power delivered.

The main control can be divided into two main sections which is the input side controller and grid side controller. While the control in grid connected power converters should have the basic function as listed below with minimum disturbances to power quality on the grid and converter, extra features such as local voltage and frequency regulation, harmonic compensation and active filter may be add on [26].

Input side controller:
- The main feature is to derive the maximum power from the input power source.
- Provide protection of the input side converter

Grid side controller:
- Grid synchronisation by matching the voltage magnitude, phase angle, and frequency on converter output and grid. This is known as grid connected mode.

- Operate on island mode upon loss of grid power supply as a microgrid.
- Control of active power generated to the grid.
- Control of reactive power transfer between power converter and grid
- Control the quality of power injected to grid
- Load sharing of two parallel converters operating on the same microgrid.

2.3 OVERVIEW OF CONTROL STRUCTURE

The control strategy of power conversion unit which is shown as main controller block in Figure 2.1 will be the main focal point of this thesis project. Figure 2.2 below illustrates the generic control system structure of power converter. This model will be the basis for control strategy implemented in this thesis and is elaborated in detail in Chapter 4 and Chapter 5. The conventional control structure for grid connected converter consists of two cascaded loop, namely:

- Current control loop (CCL)
- Voltage control loop (VCL)
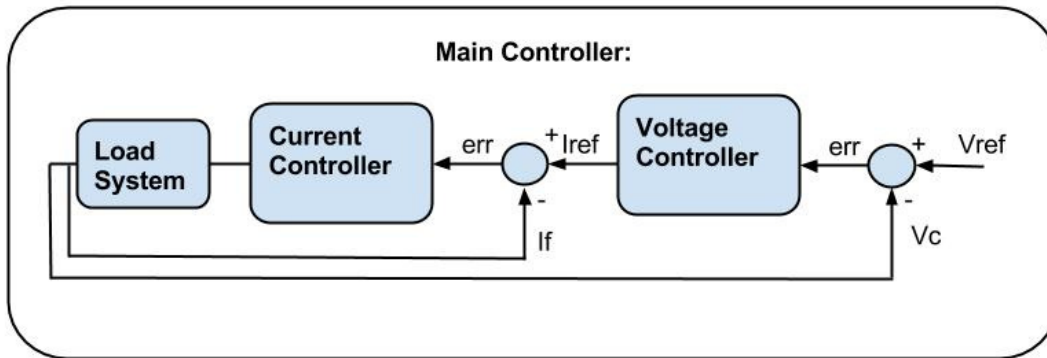
Figure 2.2: Generic block diagram of control system structure of grid connected converter

It is common to use an inner CCL to regulate the converter current and an outer VCL to regulate the converter voltage output. Cascaded control requires that the bandwidth (speed of response) increase towards the inner loop, with the CCL being faster than the VCL [27]. In certain control strategy, power control loop (PCL) is added in order to control the power delivered to the grid.

In a cascaded control structure the inner control loop has the vital role in the overall dynamic responsiveness. Thus optimal performance of CCL has been the main focus in the present control schemes development [28].

2.4 GRID FILTER TOPOLOGIES

Due to the switching effect of converter which repetitively switches on and off a DC voltage for a specific duration determined by gate signal from pulse width modulator (PWM), the output voltage is subject to a significant harmonic distortion. Detail operation of PWM and modulated output voltage are presented in section 3.4. In order for the voltage and current output from converter to achieve a defined shape and value before

entering the load system, a grid filter has to be connected between converter output and load system which in our case is grid network, as depicts in Figure 2.3. This will result in a smoother sinusoidal voltage and current with lower harmonic distortion delivered to the grid. However a precise design of grid filter is pivotal as the attenuation at the inverter's switching frequency has to be sufficient and it must not caused oscillation to the whole system [29]. Three different topologies of grid filter are elaborated below.
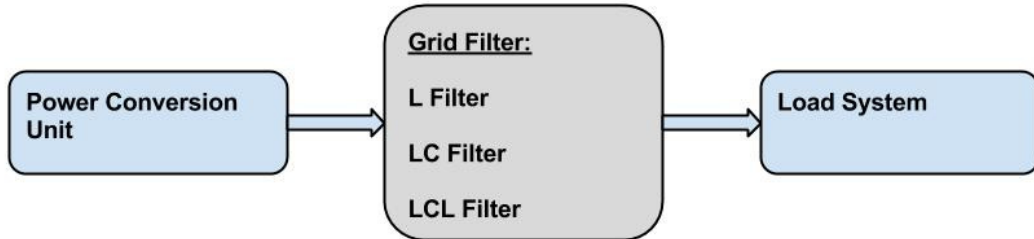
Figure 2.3: Grid filter interconnection with grid connected converter

L-Filter

The L-filter is a first order filter consists of one inductor in series with the converter and grid and shown in Figure 2.4. A common filter used due to its simplicity and trouble free from resonance issues. However the disadvantage is the size of the inductor required to reach sufficient attenuation of the current harmonics [30]. Having attenuation with 20dB/decade over the whole frequency range, this filter is suitable for converters with high switching frequency.
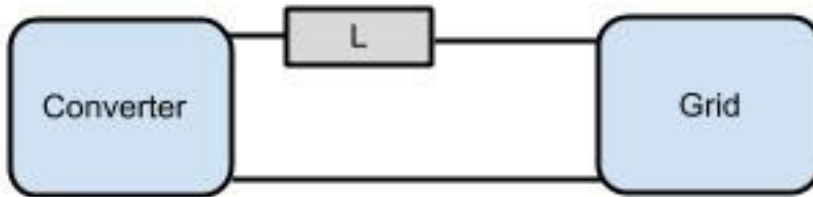
Figure 2.4: L-Filter

LC-Filter

LC-filter as depicted in Figure 2.5 is a second order filter consists of one inductor and one capacitor. It generally has a better damping behaviour than L-filter. The second order filter provides 12dB/octave of attenuation after the crossover frequency, f_c it has no gain before f_c but shows a peaking at the f_c. In grid connected converter LC-filter is not favourable as the resonance frequency of the filter is depended on the inductance value of the grid [29]. It is worthwhile to notice before LCL-filter is connected to grid. The filter configuration and characteristic can be represented by a LC-filter.
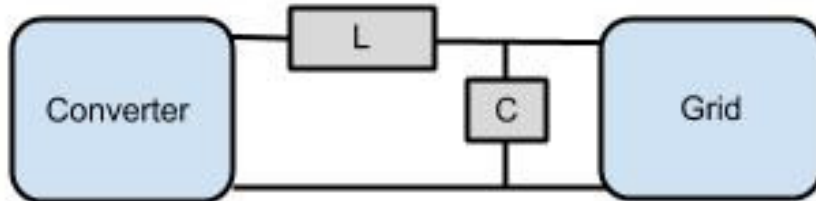
Figure 2.5: LC-Filter

LCL-Filter

In order to overcome the dependency of grid inductance in LC-filter, the third order LCL-filter in Figure 2.6 becomes a common grid filter used in industry. With attenuation of 60dB/decade for above f_c it allows lower switching frequency for the converter. It also gives better decoupling between filter, grid impedance and lower current ripple across the grid inductor. The dynamic control of inverter with LCL-filter is more complicated than L-filter. As the addtitional two poles and zeroes in LCL-filter can lead to unstability in control system, active or passive damping method is usually implemented to mitigate this issue [29]. Active damping involves an independant control mechanism often based on real time measurement or estimated value while passive damping consist of installation of additional components such as resistor, inductor and capacitor. More literature related to grid filter and damping methods can be found in [31], [32], [33] and [34].
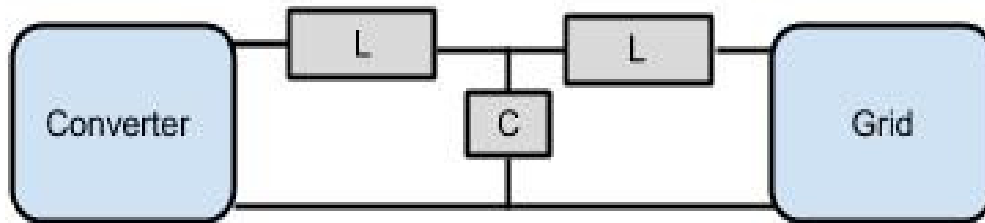
Figure 2.6: LCL-Filter

3   CONTROL SYSTEM COMPONENTS AND TOOLS

Control system of a grid connected converter is build up from the integration of several components or subsystem while the control signal can be in the form of stationary or synchronous reference frame. With the application of PI controller, design of the controller's parameter is necessary for a stable control system.

This chapter will take a comprehensive look into the various components function and methodologies in detail which consist of controller's type, controller optimization, control signal reference frames, pulse width modulator (PWM), and converter which are all widely implemented in this thesis work and industry.

3.1   TYPES OF CONTROLLER

Various types of controller exist in the industry; however hysteresis controller and proportional integral (PI) controller are the most commonly used controller and further discussed below.

3.1.1   Hysteresis Controller

Hysteresis control or sometimes named tolerance band control for current regulator can be traced in power electronic book by Ned Mohan [35]. Figure 3.1 below shows a sinusoidal reference current with an upper and lower band limit which forms the tolerance band. It can be seen that when the actual current reaches the upper band limit, T_{A-} switch is turned on (T_{A+} switch is turned off) connecting ground voltage to the load which will lead to reduction of actual current. On the other hand, when the actual current reaches lower band limit, T_{A+} switch is turned on (T_{A-} switch is turned off), hence delivering voltage V_d to load.

It is significantly indicated in the figure below that this method of control results in irregular switching frequency during the fundamental period. The switching frequency is dependant on tolerance bandwidth and the changing rate of actual current from upper to lower band limit and vice versa. While actual current rate of change is determined by the voltage level V_d and the load impedance.

However due to its fast response, hysteresis controller can be a preferable option especially in current control which required a high speed control response. In addition, hysteresis controller has its relatively distinct advantages for its simplicity of implementation and the exclusion from the need of known load parameters in controller design.
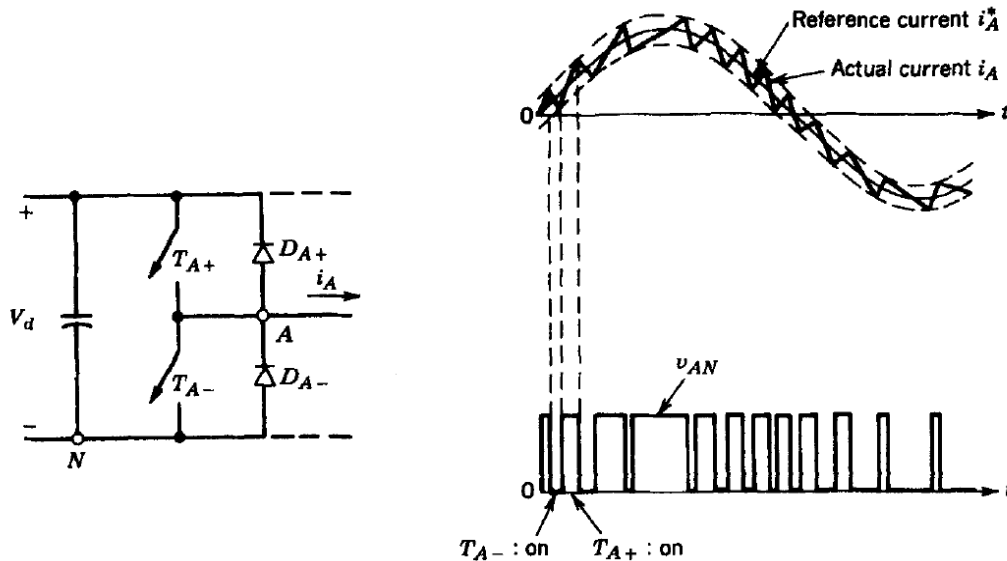
Figure 3.1: Hysteresis current control [1]

3.1.2   Proportional Integral (PI) Controller

PI controller is a linear controller and perhaps one of the most common controllers used in the industrial control system. It works on the principal of control loop feedback as depicted in Figure 3.2. The error of the reference and measured output signal is the function of the control response which will regulate the output until it matches the reference value. There are two terms namely proportional and integral action in the controller.
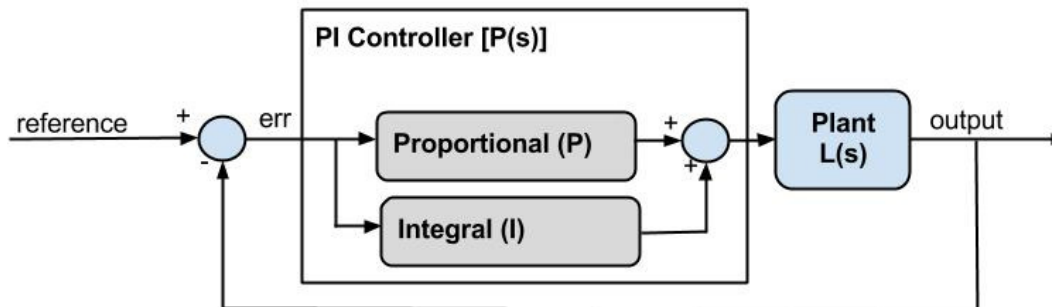
Figure 3.2: Generic system structure of PI controller

The control action of the proportional term is simply proportional to the control error. The proportional term output is given by multiplying the error by a constant K_p which is called the proportional gain constant. The equation is given by (3-1). As the error becomes larger the proportional term output of the controller is magnified to give more correction. A high K_p will produce a large change in output and may lead to system instability while a too low K_p will result in a less responsive controller to the system disturbance [36]. From Figure 3.3 it can be understood that the proportional term is a timely and fast control however it will result in a small control error in steady state [37].

22

$$U(t) = K_p \cdot err(t) \tag{3-1}$$
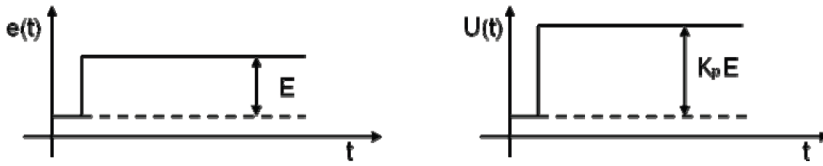
Figure 3.3: Input and output of proportional term control [37]

The main objective of integral term in PI controller is to eliminate control error in steady state. The integral control is proportional to the magnitude and duration of the error. It calculates and accumulates a continuous sum of the error signal. Thus a small steady state error will result into a large error value over time as shown in Figure 3.4. The accumulated error is then multiplied by constant K_i which is called the integral gain constant and gives the integral control output. The equation of integral term is given by (3-2). A small positive error will always lead to an increasing control output and vice versa [36]. Thus it vividly shows the advantage of integral action in eliminating steady state control error.

$$U(t) = K_i \cdot \int_0^t err(t) \tag{3-2}$$
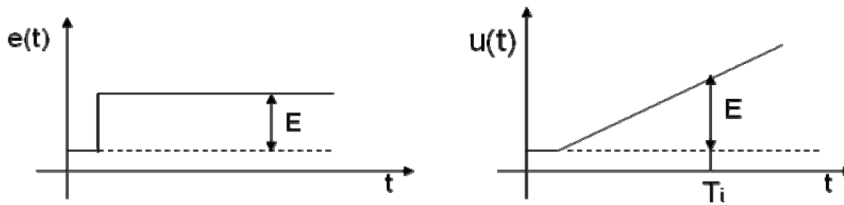
Figure 3.4: Input and output of integral term control [3]

PI controller output can be expressed as (3-3) and (3-4) below where T_i is the integral time constant and its transfer function representation as (3-5). These expressions will be important for controller tuning and system stability analysis.

$$U(t) = K_p \left(err(t) + \frac{1}{T_i} \cdot \int_0^t err(t) \right) \tag{3-3}$$

$$\text{where } K_i = \frac{K_p}{T_i} \tag{3-4}$$

$$P(s) = K_p \left[\frac{1 + T_i S}{T_i S} \right] \tag{3-5}$$

3.2 CONTROLLER OPTIMIZATION

Controller design is implementing a specific methodology to determine the parameters of the controller. Parameter of a PI controller in this context consists of the proportional gain constant, K_p and the integral time constant, T_i. Different methodologies applied on the same control system will produce a different dynamic response or more often the term specification of a control system is used. The typical specification of a control system may include attenuation of load disturbances, sensitivity to measurement noise, set-point following and robustness to model uncertainty [36]. Some of the specification of a control system is conflicting with each other, for example attenuation and sensitivity to measurement errors, while some specification may not be relevant to the control system requirement.

This section will describe one powerful technique that optimize the chosen specification that is most important to the control system while compromise on several different criteria [36]. Optimization technique has been proven to be a success in the design of PI controller and has been widely implemented in the design of control of grid connected converter. Two ubiquitous optimization approaches namely modulus optimum (MO) and symmetrical optimum (SO) are elaborated in detail below. In chapter 5 application of optimization in designing PI controller based control system will be presented in detail.

3.2.1 Modulus Optimum

The objective of Modulus Optimum (MO) approach in tuning of PI controller is to keep the modulus or absolute value of the frequency characteristic as close to unity or 0 db for the system closed loop transfer function, $G_{CL}(s)$ over a widest possible frequency range [38]. This method is popular due to its simplicity and rapid response.

MO method can be applied to control system with one or two large time constant with several small time constants or simply with only several small time constants. It is proven that small time constant does not contribute to the overall control behaviour thus it can be added together and represented by an equivalent time constant [10-2]. The standard form of the control system transfer function is achieved by cancelling the largest time constant and setting the closed loop gain higher than unity for highest frequency possible [39]. Below is an example of a system with one large time constant and several small time constants. System with different types of time constants may not be able to optimize with PI controller but could be managed with integral (I) controller or proportional-integral-derivative (PID) controller. Although these systems are not discussed in this thesis, several standard forms with its tuning formula are given in Appendix B.

Assume the transfer function of plant system block in figure 3.2 is represented by (3-6) shown below with one large time constant, T_a and three small time constants, T_b, T_c and T_d. By combining the small time constants into one equivalent time constant, T_e the transfer function can be simplified as (3-7). With reference to PI controller transfer function in (3-5), the system open loop transfer function, $G_{OL}(s)$ can be written as (3-9).

$$L(s) = \frac{K_s}{(1+T_a S)(1+T_b S)(1+T_c S)(1+T_d S)} \qquad (3\text{-}6)$$

$$L(s) = \frac{K_s}{(1 + T_a S)(1 + T_e S)} \qquad \text{where } T_a > T_e \qquad (3\text{-}7)$$

Where $T_e = T_b + T_c + T_d$ $\qquad\qquad$ (3-8)

$$G_{OL}(s) = K_p \left[\frac{1 + T_i S}{T_i S} \right] \cdot \frac{K_s}{(1 + T_a S)(1 + T_e S)} \qquad (3\text{-}9)$$

By applying the zero pole cancellation of the dominating pole of the system and optimizing absolute value to unity as in (3-10) and (3-11), the $G_{OL}(s)$ and $G_{CL}(s)$ can be simplified into a standard form as in (3-12) and (3-13).

$$T_i = T_a \qquad\qquad (3\text{-}10)$$

$$K_p = \frac{T_a}{2 K_s T_e} \qquad\qquad (3\text{-}11)$$

$$G_{OL}(s) = \frac{1}{2 T_e S} \cdot \frac{1}{(1 + T_e S)} \qquad\qquad (3\text{-}12)$$

$$G_{CL}(s) = \frac{1/2 T_e^2}{S^2 + \frac{1}{T_e} S + \frac{1}{2 T_e^2}} \qquad\qquad (3\text{-}13)$$

Comparing (3-13) to the general equation of second order transfer function (3-14), it can be seen that the system results in frequency of natural oscillation,

$$\omega_o = \frac{1}{\sqrt{2 T_e}} \text{ and damping factor } \zeta = \frac{1}{\sqrt{2}} .$$

It is clearly shown that by using the same approach the system response will always corresponds to the same values of ω_o and ζ. However the controller can always be adjusted to the required crossover frequency, f_c by changing K_p [39]. The crossover frequency is always chosen to be one to two times smaller than switching frequency, f_{sw} to avoid switching noise interference.

$$G_{CL}(s) = \frac{\omega_o^2}{S^2 + 2\zeta\omega_o S + \omega_o^2} \tag{3-14}$$

3.2.2 Symmetrical Optimum

Symmetrical optimum (SO) approach for controller tuning method is to produce maximum phase margin (PM) for the closed loop system [40]. PM maximisation at given frequency enables higher delay tolerance which is important for systems consist of delay. This method optimizes the control system response corresponding to disturbance input [39]. The main advantage of this method is due to its well developed tuning rule and has good disturbance rejection relative to other methods [41]. Besides for system transfer function which has an integrator element will not be able to use MO approach. As the system integrator elements combined with the integrator element from PI controller will lead to oscillation of the controlled variable [30]. In this case SO approach can be implemented.

The derivation of PI controller parameters based on the system transfer function as assumed in (3-6) is lengthy and involves a number of approximations and simplifications. Thus, it is not included in this thesis, however basic approach and extended approach of tuning by SO can be found at [42] and [43] respectively. The well structured SO tuning rule of PI controller parameters for various types of system transfer function is well documented in the book PID controllers tuning by Åstrom and Tore [36] and presented in Appendix B.

For a plant with transfer function (3-7), PI controller parameters can be expressed as (3-15) and (3-16) below:

$$T_i = \sigma^2.T_e \tag{3-15}$$

$$K_p = \frac{T_a}{\sigma K_s T_e} \tag{3-16}$$

While for system transfer function with one integrator and one time constant (3-17), as given in example below, PI controller parameters can be expressed as (3-18) and (3-19).

$$L(s) = \frac{K_s}{S(1+TS)} \tag{3-17}$$

$$T_i = \sigma^2.T \tag{3-18}$$

$$K_p = \frac{1}{\sigma K_s T} \tag{3-19}$$

Parameter σ above is defined as the symmetrical distance between $1/T_i$ and $1/T_\alpha$ to crossover frequency, f_c and for conventional SO tuning σ is set at 2. By increasing σ the system will have a better damping and higher phase margin, PM but its response will become slower [39]. Therefore controller's parameter selection will have a compromising effect in the system performance. The recommended value of σ is between 2 and 4 [40].

3.3   REFERENCE FRAMES IN CONTROL SIGNAL

In many ways, same methodologies in control of grid connected converter and control of motor drive are being implemented due to their similarity. For the control structure of reference frames, three possible structures have been documented in detail from previous study, namely the stationary *abc* reference frame, stationary *αβ* reference frame and synchronous *dq* reference frame [11]. A graphical representation of the three reference frames is given by Figure 3.5.
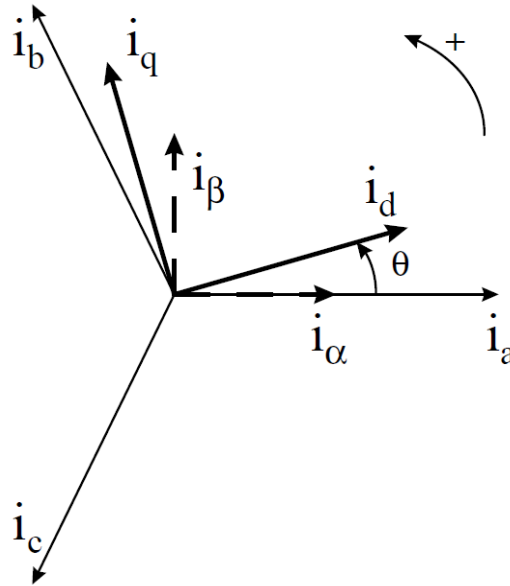
Figure 3.5: Two phase signal with orthogonal axis in (αβ) stationary frame and (dq) synchronous frame in relation with three phase signal [44]

The fundamental three phase voltage and current can be transformed into different reference frame throughout the entire control loop. The description of each control structure and its transformation method will be elaborated in sections below while the implementation is comprehensively documented in Chapter 4. Industry and researchers have proven control in different reference frame will achieve the same control objective. However there will be differences in the control responses and stability which will be discussed further in Chapter 6 where simulation results of different control methods are presented.

3.3.1   Stationary *abc* Reference Frame

The stationary *abc* reference frame or natural frame structure is the fundamental and most direct control structure where no transformation is required on the three phase current or voltage. Three controllers are necessary in this case with one for each phase.

3.3.2   Stationary *αβ* Reference Frame

A three phase signal can be transformed into two phase orthogonal system in stationary frame where both axes are locked in position by using Clarke transformation or more often referred as αβ-transformation. This mathematical transformation is widely utilised to simplify analysis of three phase circuits. One of the distinct advantages working with two phase signal is that only two instead of three controllers are required hence reducing the power consumption in digital signal processors or micro-controllers [11]. The transformation is shown in matrix equation (3-20), (3-21) and (3-22) below [45]:

$$\begin{bmatrix} I_\alpha \\ I_\beta \\ I_\gamma \end{bmatrix} = \begin{bmatrix} 1 & -\frac{1}{2} & -\frac{1}{2} \\ 0 & \frac{\sqrt{3}}{2} & -\frac{\sqrt{3}}{2} \\ \frac{1}{2} & \frac{1}{2} & \frac{1}{2} \end{bmatrix} \begin{bmatrix} I_a \\ I_b \\ I_c \end{bmatrix} \tag{3-20}$$

In a balance three phase current system $I_a + I_b + I_c = 0$, which will results in $I_\gamma = 0$. Thus, two of the phase current is sufficient to compute αβ-component. This simplifies the transformation into matrix equation shown as below [34]:

$$\begin{bmatrix} I_\alpha \\ I_\beta \end{bmatrix} = \begin{bmatrix} 1 & 0 \\ \frac{1}{\sqrt{3}} & \frac{2}{\sqrt{3}} \end{bmatrix} \begin{bmatrix} I_a \\ I_b \end{bmatrix} \tag{3-21}$$

Inverse Clarke transformation is shown below for reference:

$$\begin{bmatrix} I_a \\ I_b \\ I_c \end{bmatrix} = \begin{bmatrix} 1 & 0 \\ -\frac{1}{2} & \frac{\sqrt{3}}{2} \\ -\frac{1}{2} & -\frac{\sqrt{3}}{2} \end{bmatrix} \begin{bmatrix} I_\alpha \\ I_\beta \end{bmatrix} \tag{3-22}$$

3.3.3   Synchronous *dq* Reference Frame

Park transformation or more often referred as dq-transformation transforms three phase signal into a two phase orthogonal system in synchronous frame where the axis system is rotating on a reference frequency. Thus this transformation will require a reference phase angle, θ. Method describes here divides the dq-transformation process into two parts for easier understanding. Firstly, a three phase signal is transformed into two phase signal using αβ-transformation as shown in the previous section and secondly, to use dq-transformation to obtain the dq-component signal which is shown by the matrix equation (3-23) and (3-24) below [45]:

$$\begin{bmatrix} I_d \\ I_q \end{bmatrix} = \begin{bmatrix} \cos\theta & \sin\theta \\ -\sin\theta & \cos\theta \end{bmatrix} \begin{bmatrix} I_\alpha \\ I_\beta \end{bmatrix}$$

(3-23)

Inverse Park transformation is shown below for reference:

$$\begin{bmatrix} I_\alpha \\ I_\beta \end{bmatrix} = \begin{bmatrix} \cos\theta & -\sin\theta \\ \sin\theta & \cos\theta \end{bmatrix} \begin{bmatrix} I_d \\ I_q \end{bmatrix}$$

(3-24)

3.4 PULSE WIDTH MODULATION (PWM)

Being one of the most widely implemented modulation techniques, PWM is based on width of the pulse generated with respect to the control signal information. In electrical voltage regulation, the control signal is often a sinusoidal wave. There are several methods which is commonly applied in PWM modulation such as carrier based PWM, space vector modulation (SVM) and random PWM. Carrier based PWM is elaborated below due to its implementation in this thesis project while the differences of other methods can be found in [46].

Carrier based PWM is the fundamental and most common way to modulate switching signals. The control signals which are three sinusoidal waves representing phase voltage in this particular application are compared with the carrier signal which is usually a triangular wave at higher frequency. During the period when control signal is larger than carrier signal, switch is turned on and vice versa which can be seen in Figure 3.6. Each of the phases will have its switching independent and producing its voltage output which on average form a fundamental sinusoidal waveform. This average voltage output can be controlled by adjusting the control signal.

3.5 CONVERTER (TIME DELAY)

A converter which converts voltage from AC-DC or DC-AC with reference to switching gate signal from modulator can be considered as a voltage transformer in control system. The process flow as illustrated in Figure 3.7, from the input of voltage reference to modulation of gate switching signal and the switching by converter to achieve the corresponding converter voltage output. A converter can only give a limited range of voltage vector and thus only the average voltage output over a switching period will be equalled to the reference voltage. As such, it involves a significant delay from the time when a reference voltage is given until it is applied on the load. This time delay has to be taken into account in system design and it is often referred as switching time delay, T_{sw} and can be represented as $e^{-T_{sw}S}$ in Laplace-domain.
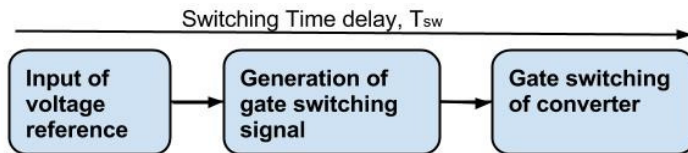
Figure 3.6: Flow chart of converter switching time delay

As the term is not a rational function, it is not possible to determine an algebraic solution for control parameters. It can be approximated to a rational expression as in (3-26) by using Taylor series for exponential function expanded to first order component as shown (3-25) below [47]:

$$e^x = \sum_{n=0}^{\infty} \frac{x^n}{n!} = 1 + x + \frac{x^2}{2!} + \frac{x^3}{3!} + \frac{x^4}{4!} + \ldots\ldots \tag{3-25}$$

.

$$e^{-T_{sw}S} = \frac{e^{\frac{-T_{sw}S}{2}}}{e^{\frac{+T_{sw}S}{2}}} \approx \frac{1 - \frac{T_{sw}S}{2}}{1 + \frac{T_{sw}S}{2}} \tag{3-26}$$

In order to eliminate the numerator of dynamics, the numerator can be expanded to order of zero as in (3-27).

$$e^{-T_{sw}S} \approx \frac{1}{1 + \frac{T_{sw}S}{2}} \tag{3-27}$$

Subsequently, the converter transfer function can be expressed as (3-28) with a converter time delay represented as T_α. In this project it is important to note that assumption where the converter time delay, T_α, to be half of the switching period, T_{sw} has been made, with other existing delays which have not been discussed here is assumed to be included in this assumption.

$$C(s) = \frac{1}{1 + T_\alpha S} \qquad\qquad \text{where } T\alpha = 0.5 \text{ Tsw} \tag{3-28}$$
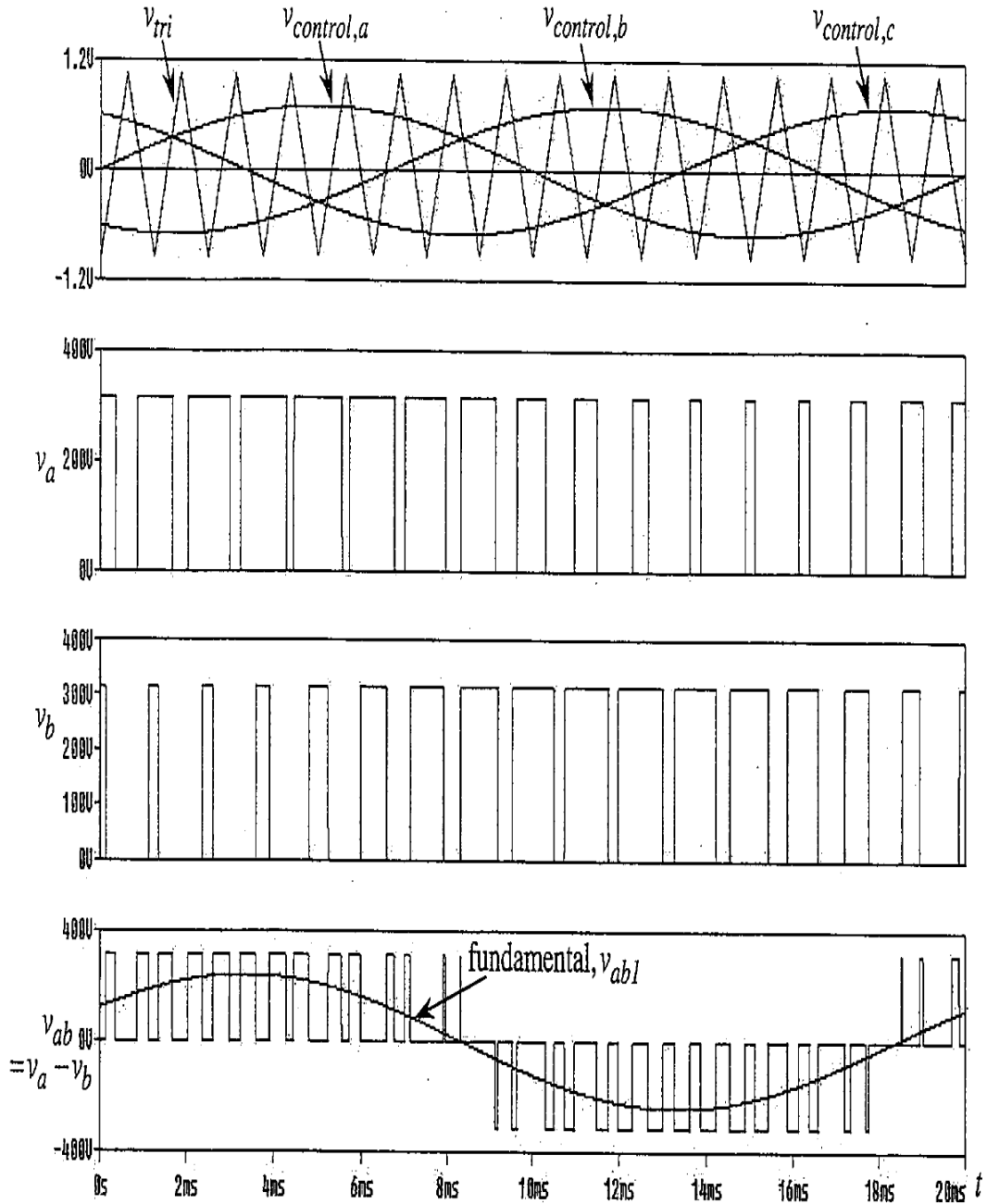
Figure 3.7: Three-phase PWM with triangular carrier signals and output voltage waveform [27]

4 CONTROL SYSTEM STUCTURE AND STRATEGY

In converting DC power to AC power, two vital components that need to be controlled are the three phase AC voltage and current. The parameters of the voltage and current that require precise control are magnitude, frequency and phase angle of the respective components which will eventually determined the amount of power delivered to grid. These controllers are conventionally designed in the form of cascaded loop control structure.

This chapter starts with introduction of the whole control structure in detail which consists of inner current control loop and outer voltage control loop. In the following sections, comprehensive structure and various strategies for current controller and voltage controller are presented. These include implementation of different controller's type and control signal reference frame.

4.1 CONVERTER CONTROL SYSTEM STRUCTURE

This thesis utilized the conventional cascaded control structure and it is vital for reader to have a good understanding of this system structure before proceeding further. As overview presented in Chapter 2, the cascaded control structure used consist of one inner and one outer control loop. The control system design will commence from the inner control loop to the outer control loop.

Figure 4.1 illustrates the converter control system structure for grid synchronization. Upon a successful synchronization, the converter control will switch to normal operation control system. The only difference between grid synchronization and normal operation control system structure is the voltage reference input to the controller. Instead of using grid voltage as reference, normal operation control will generate voltage reference based on the active and reactive power demand. This reference voltage is often generated by an additional power controller. Normal operation control is not covered in this thesis however a comprehensive presentation can be found in [19].

For grid synchronization control, the outer VCL uses the filter capacitor voltage, V_c to compare with reference voltage, V_{ref} where in this case is the grid voltage, V_g. The voltage error passing through the voltage controller will generate a current reference signal, I_{ref}. Subsequently, inner CCL uses generated I_{ref} to compare with converter output current, I_f. The current error via current controller will generate required converter voltage output, V_e. The required converter voltage output, V_e through a PWM modulator will in turn generate the corresponding gate switching signal to converter.

While current and voltage control system design can be categorized by the different types of controller applied such as hysteresis controller and PI controller, it can be further subdivided into different control signal reference frame namely stationary reference frame and synchronous reference frame. Each of the different approach inclusive of its theory and structure is presented in sections below while system modelling and controller tuning will be presented in Chapter 5.
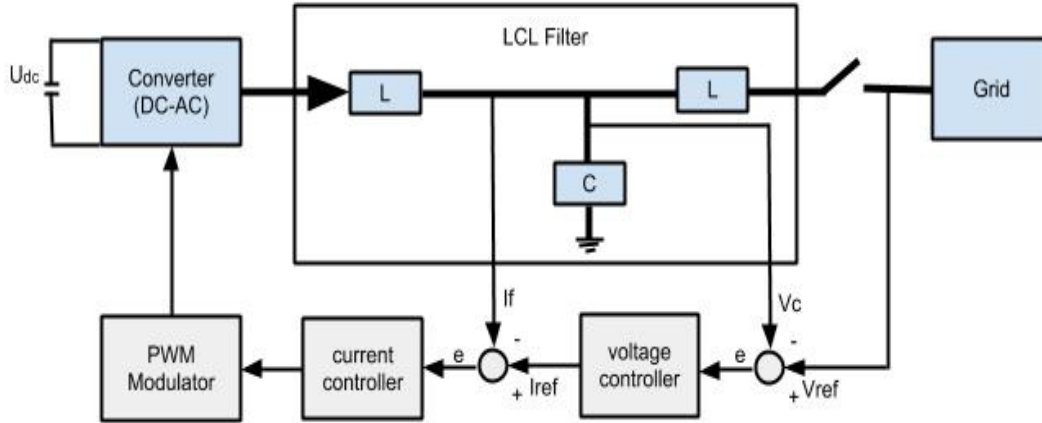
Figure 4.1: Control system structure of grid connected converter

4.2   CURRENT CONTROL STRATEGY

Current control techniques can be generally categorized in three groups consisting of hysteresis control, linear current control and predictive control [48]. The main objectives of a current controller can be listed as below. It has been a mammoth challenge to meet these objectives and huge effort has been put into research on this topic [49]:

- To achieve zero steady state error.
- Precise tracking of reference current during transient changes which requires a control system with high bandwidth for good dynamic response.
- Limiting peak current to prevent overloading.
- Minimising harmonics other second order effects of inverter operation

Hysteresis control and linear current control using PI controller in stationary and synchronous frame will be the three current control strategies discussed in this thesis. For verification and comparison purpose, it is assumed generation of current reference signal, I_{ref} is a pre defined constant value. The utmost objective is to observe the response of converter output current, I_f in different control methods and design the parameters of PI controller that gives a fast and accurate performance of converter output current, I_f.

4.2.1   PI Controller in Stationary *αβ* Reference Frame

Implementation of closed loop PI controller is one of the common techniques in controlling current. This approach has a fixed converter switching frequency which results in known output current harmonics content [50]. However, a proper design of PI controller parameters is vital for satisfactory control performance. One of the significant disadvantages of this method is where it requires the known parameters of load circuits and a lengthy modelling of circuit and controller tuning methods. Tuning of PI controller's parameters and modelling of converter circuit together with feed forward compensation technique are discussed thoroughly in Chapter 5.

By choosing the stationary *αβ* reference control frame, three phase AC signal which is 120º apart has to be transformed into two phase orthogonal signal using Clarke's transformation (αβ-transformation) as presented in section 3.3.2. It is important to note

that with the implementation of two phase signal, it requires only two PI controllers in each phase instead of three. Figure 4.2 below illustrates the general control structure of PI controller in stationary reference frame.

Current error between I_{ref} and I_f will serve as input to the PI controller, while the output signal from PI controller will be transformed back to three phase signal. This three phase signal will be the input into pulse width modulator (PWM) for generating converter's gate signals.
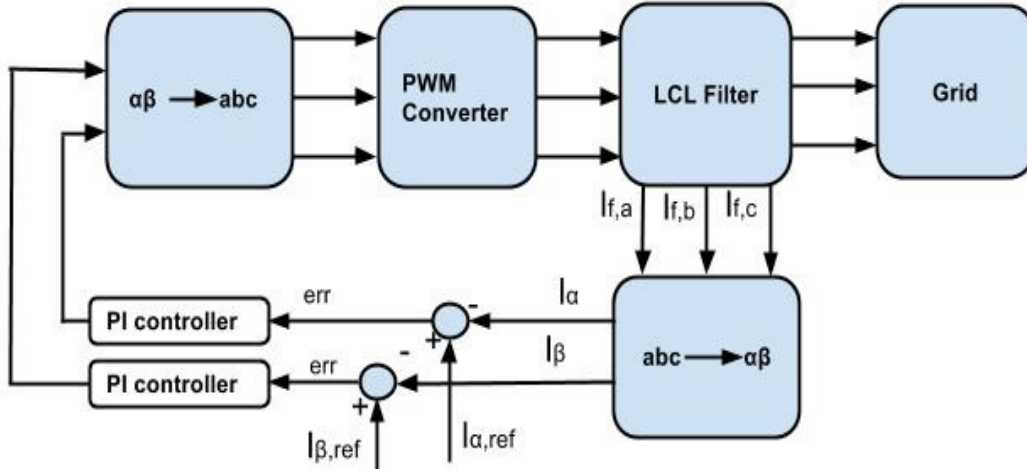
Figure 4.2: Current control with PI controller in stationary $\alpha\beta$ reference frame

However it is important to note that in this approach the input current signal to PI controller is an alternate current (AC) signal instead of direct current (DC) signal. Thus, PI controller is not sufficient to track the rotating current references and results in steady state error. This limitation can be overcome by implementation of synchronous reference frame [51] as elaborated below.

4.2.2   PI Controller in Synchronous *dq* Reference Frame

In general the approach of this method is similar to section 4.2.2. The main difference is with the usage of synchronous reference frame instead of stationary reference frame. This involves an additional phase angle parameter extracted from chosen reference frequency as can be seen in Figure 4.3 which shows the general control structure of PI controller in synchronous reference frame.

Current control loop with PI controller is commonly, designed to be in synchronous frame as the controller will be working with DC values in steady state [52]. By using Park's transformation (dq-transformation), two phase AC signal in stationary frame can be transformed into two phase DC signal as presented in section 3.3.3. This transformation required a phase angle, of chosen frequency where θ is usually extracted by phase locked loop (PLL) as depicted in figure 4.3. This thesis utilize grid voltage phase angle as reference for the synchronous frame. Design of PLL is not within the scope of this thesis however relevant information can be found at [52], [28], [30].

Current error between I_{ref} and I_f will serve as input to the PI controller, while the output signal from PI controller will be transformed back to three phase signal. This three phase signal will be the input into pulse width modulator (PWM) for generating converter's gate signals. Feed forward compensation of the coupling components effects will be added for higher satisfactory performance. Detailed derivation of coupling term and structure of feed forward compensation are presented in section 5.1.1 while results and simulation of this control method is presented in Chapter 6.
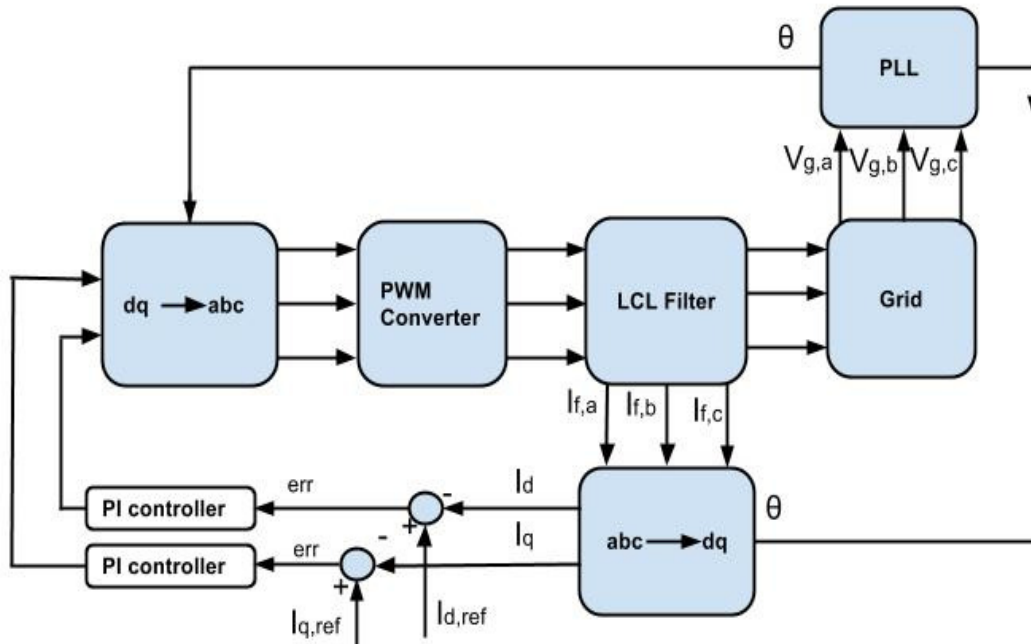
Figure 4.3: Current control with PI controller in synchronous *dq* reference frame

4.2.3   Hysteresis Controller in Stationary *abc* Reference Frame

Hysteresis controller is one of the preferred controllers in current control loop due to its high dynamic response as required for inner control loop of cascaded structure discussed in section 4.1. One of the possible implementation with fixed band hysteresis controller in stationary *abc* frame is depicted in Figure 4.4.

This method is considered to be one of the simplest to implement as it does not require any signal transformation and parameters of load system are not required to be known in designing the control system unlike PI controller which involves heavy analysis. However this approach requires three identical hysteresis controllers, one more than the other reference frame control as discussed in section above with the use of PI controllers. The only parameter that will be changed for observation is the tolerance band. Different tolerance band setting will be tested in simulation for discussion in Chapter 6.
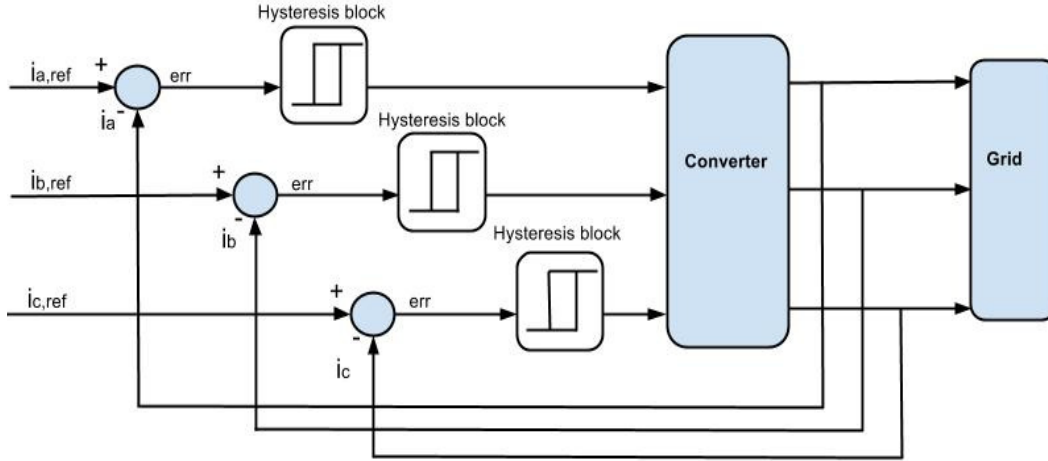
Figure 4.4: Current control with hysteresis controller in stationary *abc* frame

4.3 VOLTAGE CONTROL STRATEGY

Voltage control loop is the outer loop of the cascaded control structure described in section 4.1. The main objective of the voltage controller is to control the voltage across filter capacitor, V_c towards reference voltage which is the grid voltage, V_g in this implementation. During grid synchronization, prior to establishment of grid network connection, three parameters of the controlled voltage are required to match with the grid voltage within specified error tolerance:

- Voltage magnitude
- Voltage frequency
- Voltage phase angle

In the approach of this thesis, it is important to note that the DC link voltage source converter is assumed to have an unlimited constant voltage source. Thus control algorithm for DC link voltage is not in the scope while all it needs here is an algorithm to control the AC voltage across the filter capacitor with reference to grid AC voltage. The output of the voltage controller will be the reference current for current control loop as discussed in section 4.2. Thus in order to conduct a reliable study on the differences between several voltage control strategies, one common current control method has to be implemented on all voltage control strategies. In this project, current control with PI controller in synchronous *dq* reference frame as presented in section 4.2.2 is chosen to be common model.

The voltage control structure design is primarily utilizing PI controller while the control principal are divided into two. In the first category the magnitude, frequency and phase angle of sinusoidal voltage are being controlled together via stationary and synchronous reference frame similar as in current control structure. While the second control principal sees a separation of control in voltage magnitude from voltage frequency and phase angle. All the different methodologies are further elaborated in sections below.

4.3.1 PI Controller in Stationary *αβ* Reference Frame

This voltage control strategy controls all three voltage parameters together and it is similar to the current control strategy discussed in section 4.2.1 where control signals operate in stationary αβ reference frame with the use of Clarke's transformation.

Voltage error between filter capacitor voltage, V_c and grid voltage, V_g which is the reference voltage is fed into PI controller as depicted in Figure 4.5. The output of the PI controller will be the current reference fed into current control block which is representing the current control method as in Figure 4.3 where further transformation into synchronous dq reference frame for current control is required. This cascaded control structure involves two different reference frames. The output signal from current control will be transformed back to three phase signal. This three phase signal will be the input into pulse width modulator (PWM) for generating converter's gate signals.

Sharing the disadvantage due to stationary αβ reference frame, this method requires proper design of PI controller parameters for satisfactory control. Tuning of PI controller's parameters and modelling of converter circuit together with feed forward compensation technique are discussed thoroughly in chapter 5. It is worthwhile to note that the PI controller is tracking the sinusoidal error signal which may results in steady state error.
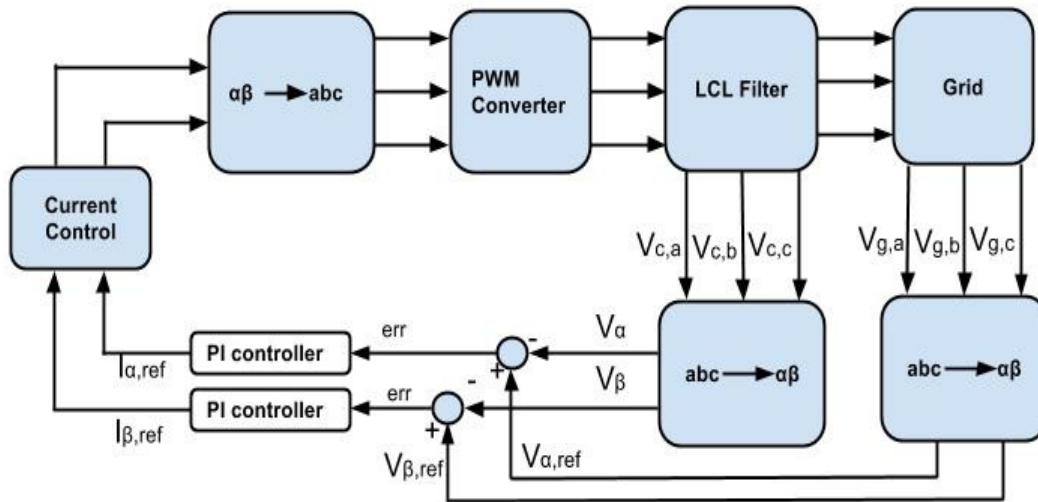
Figure 4.5: Voltage control with PI controller in stationary *αβ* reference frame

4.3.2 PI Controller in Synchronous *dq* Reference Frame

The approach of this method is largely the combination of the voltage control structure in section 4.3.1 and control signal reference frame in section 4.2.2. As illustrated in Figure 4.6, a PLL is used to extract the reference phase angle, θ for the purpose of Park's transformation.

The filter capacitor voltage, V_c and grid voltage, V_g will be first transformed into synchronous dq reference frame before taking the error of it as input to PI controller.

Here the input to the PI controller is in DC value unlike in section 4.2.2 thus allowing precise error tracking. Output from PI controller will be the current reference fed into current control block which is representing the current control method as in Figure 4.3 which was chosen as the common current control method for voltage control study. As the control signal is in the same reference frame with current control block, no further transformation is required. The output signal from current control will be transformed back to three phase signal. This three phase signal will be the input into pulse width modulator (PWM) for generating converter's gate signals.

As suggested in previous section, feed forward compensation of the coupling term is added for performance enhancement. Detailed derivation of coupling term and structure of feed forward compensation are presented comprehensively in Chapter 5, while results and simulation of this control method is presented in Chapter 6.
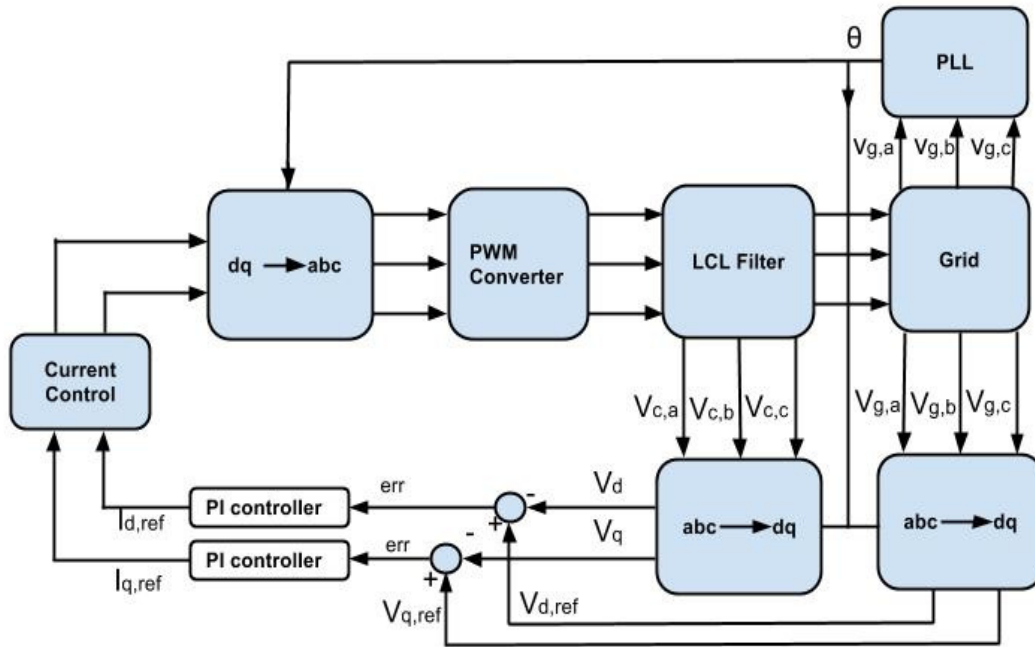
Figure 4.6: Voltage control with PI controller in synchronous *dq* reference frame

4.3.3 Magnitude and Frequency-Phase Angle Controller

The significant difference of this strategy from the above is the separation in control of voltage magnitude and control of voltage frequency-phase angle. The principal of this approach is to separately control the two axis of filter capacitor current which will in turn determine the voltage across the filter capacitor. It will utilize two PI controllers in its implementation similar with previous control methodologies. The control structure is shown in Figure 4.7.

All three of the voltage parameters magnitude, frequency and phase angle have to be extracted from the filter capacitor voltage, V_c and grid voltage, V_g as input to the controller. Voltage magnitude and phase angle can be derived from the conversion of

three phase signal into two phase signal using Clarke's transformation as presented in section 3.3.2 and subsequently converting the two phase cartesian form signal into polar form. Voltage frequency can be extracted with the use of phase locked loop (PLL).
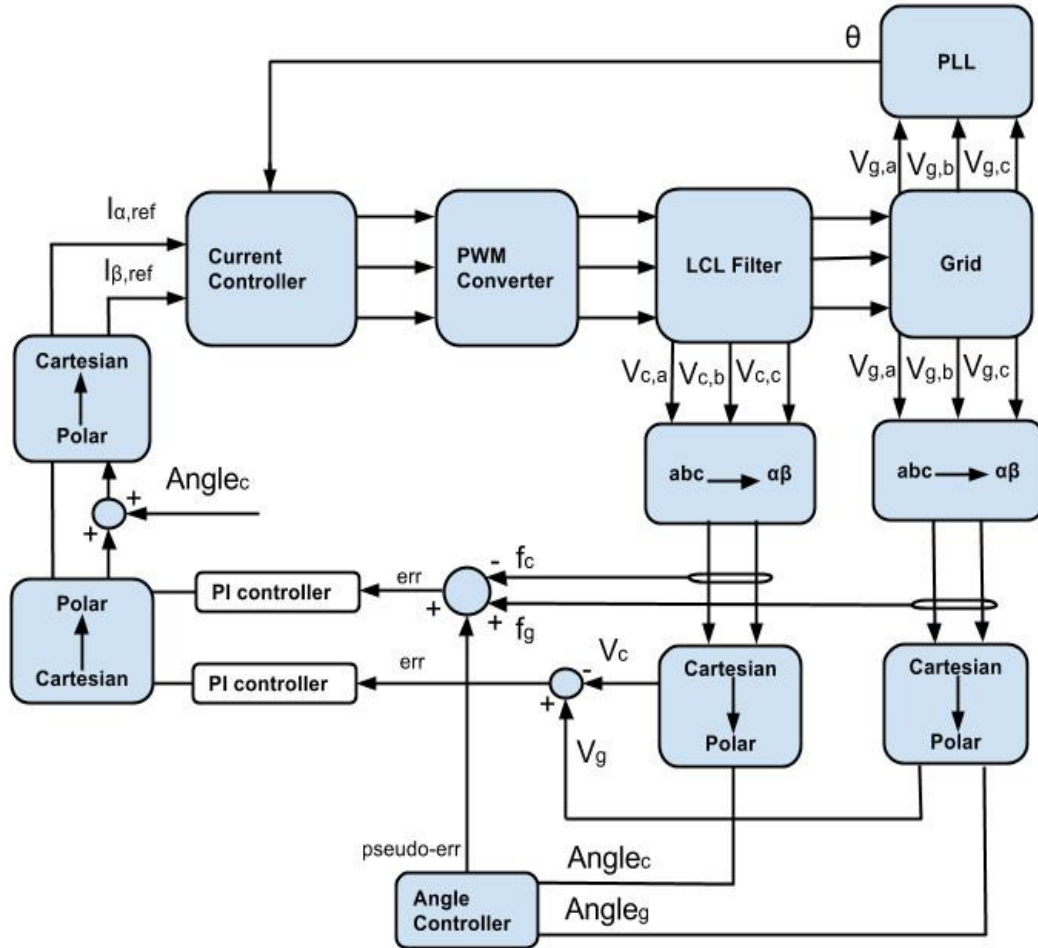
Figure 4.7: Voltage magnitude and frequency-phase angle control with PI controller in synchronous *dq* reference frame

Voltage magnitude control

Grid voltage, V_g and filter capacitor voltage, V_c magnitude are being compared to generate an error as an input to a PI controller. The output of this controller will determine the magnitude of the filter capacitor current, I_c. A phase of 90° is added to the output for it to lies at the Y-axis, as it is known that the current of a capacitor is leading its voltage by 90°. This can be seen clearly in the phasor diagram depicted in Figure 4.8 below. The relationship between the voltage and current of a capacitor is given as in (4-1). In this way, we know that magnitude of capacitor voltage can be controlled by adjusting the magnitude of current flowing into the capacitor.

$$V_c = I_c \cdot X_c = I_c \cdot \frac{1}{j\omega C}$$

(4-1)
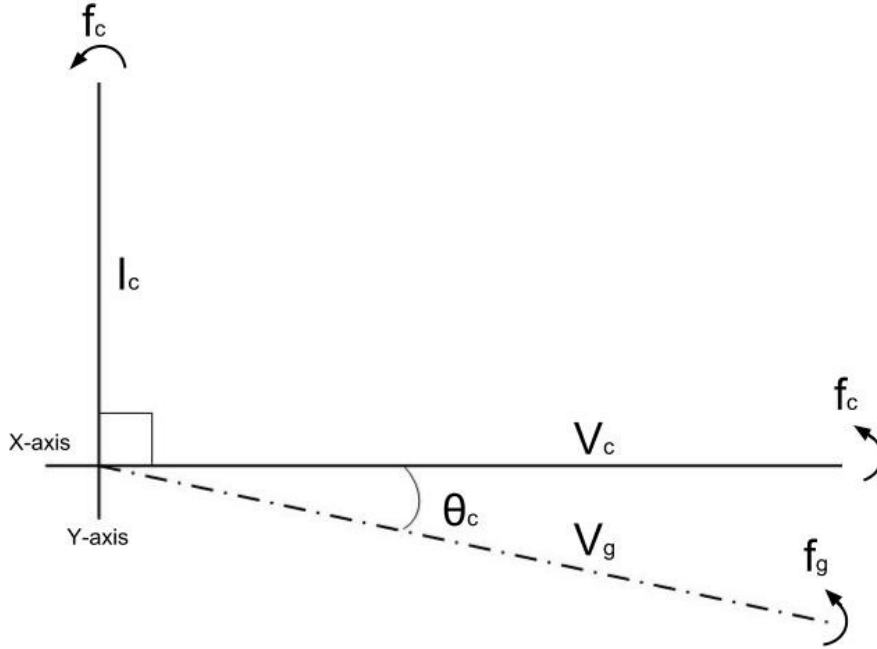
Figure 4.8: Phasor diagram of filter capacitor current and voltage with grid voltage

Frequency-Phase angle control

While we have managed to control the voltage magnitude, another controller has to be tasked to control the voltage frequency and phase angle of filter capacitor to match with the grid voltage before synchronization can take place. Both frequency and phase angle are dependant and can be determined by the relationship as in (4-2). Where θ_c is the phase angle difference between V_c and V_g. Here angle of V_g is taken as a reference angle. f_{cf} and f_g are respectively the frequency of filter capacitor and grid voltage and Δt is the time shift.

$$\theta_c = 360° \cdot \left(f_{cf} - f_g \right) \cdot \Delta t \tag{4-2}$$

It can be seen in Figure 4.8 that by introducing a small current reference at the axis of V_c also referred as X-axis, the phase angle of I_c together with the dependant 90° lagging V_c will change. This change is effectively a change of capacitor frequency, f_{cf} as given by (4-2) with the rate of change of phase angle, θ_c depending on f_{cf} since f_g is fixed. With this principal, we are able to control the voltage frequency. Referring to Figure 4.7, error of f_{cf} and f_g is fed into a PI controller and the output is the current reference of the X-axis which will determine the filter capacitor voltage frequency, f_{cf}.

However at this stage, we have no control of the phase angle θ_c between V_c and V_g. Theoretically for successful grid synchronization θ_c has to be within error tolerance besides having a frequency within error tolerance. Thus a phase angle controller as shown in Figure 4.7 is added where the output of angle controller is a pseudo-error to adjust either to increase of decrease f_{cf} in order to control θ_c. The principal of the angle controller is illustrated by the flow chart in Figure 4.9. Whenever θ_c falls out of the specified error tolerance, angle controller will issue a pseudo-error output to manipulate

f_{cf}. Once θ_c manage to be within the specified error tolerance, angle controller will stop giving output and the PI controller will be purely controlling f_{cf}. The parameters to be set for the angle controller are error limit and pseudo-error value which responses vary in different load system.
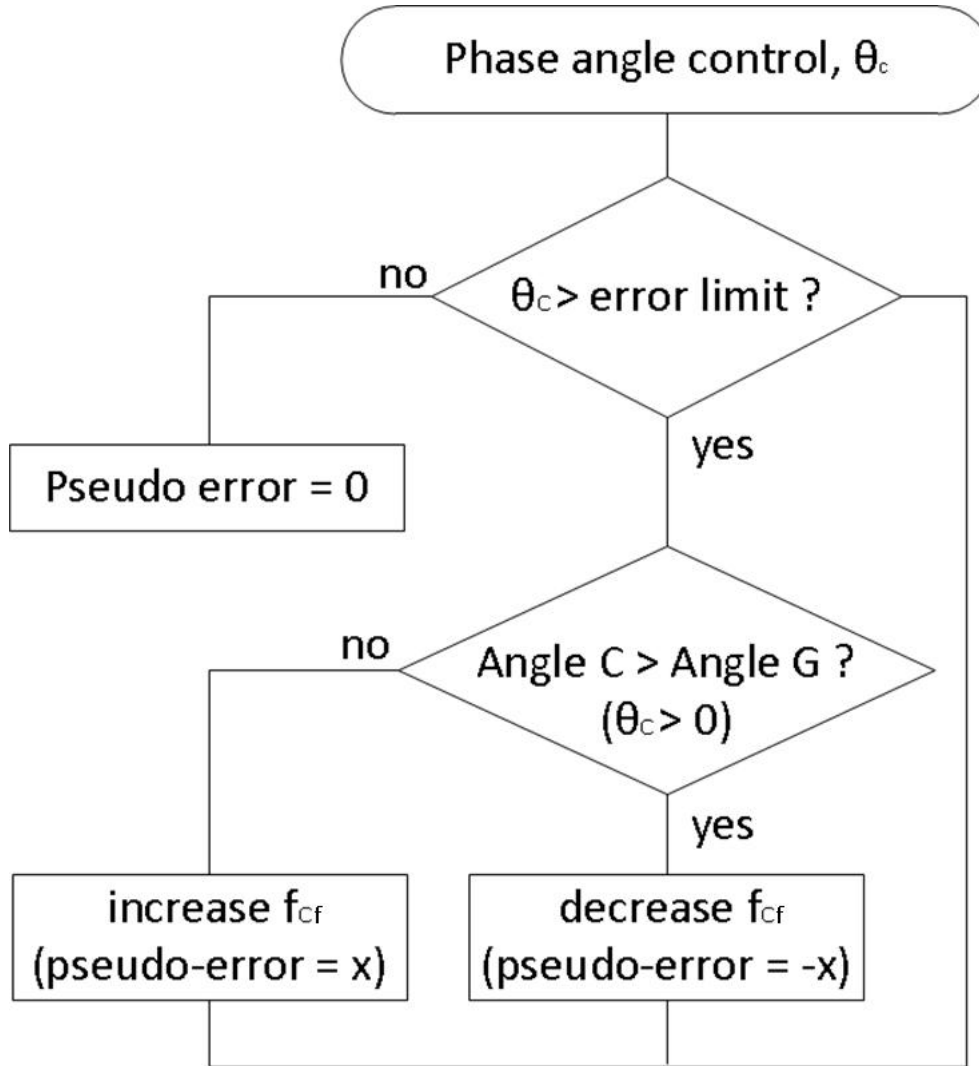
Figure 4.9: Flow chart of phase angle controller

5 CONVERTER DESIGN AND ANALYSIS

Converter design and modelling is the main subject of discussion in Chapter 5. This chapter consist of two major subtopics. It starts with the mathematical modelling of the LCL grid filter together with the implementation of feed forward compensation to eliminate cross coupling elements in synchronous reference frame. Second section presents the voltage and current controller tuning methods by optimization and bode diagram analysis was carried out to ensure the dynamic response and stability of the system is acceptable.

5.1 MODELLING OF CONVERTER WITH LCL FILTER AND TRANSFER FUNCTION REPRESENTATION

Grid filter topologies described in section 2.4 are an ideal filter where resistance has been neglected for easier understanding. Practically in each branch of the inductor and capacitor consists of a resistor. For design simplification purpose, the resistance for capacitor is assumed to be negligible due to the relatively small resistance [52]. Figure 5.1 below depicts a schematic diagram of a single phase LCL filter connected to converter. The other two phases are identical hence it is not shown in diagram below.
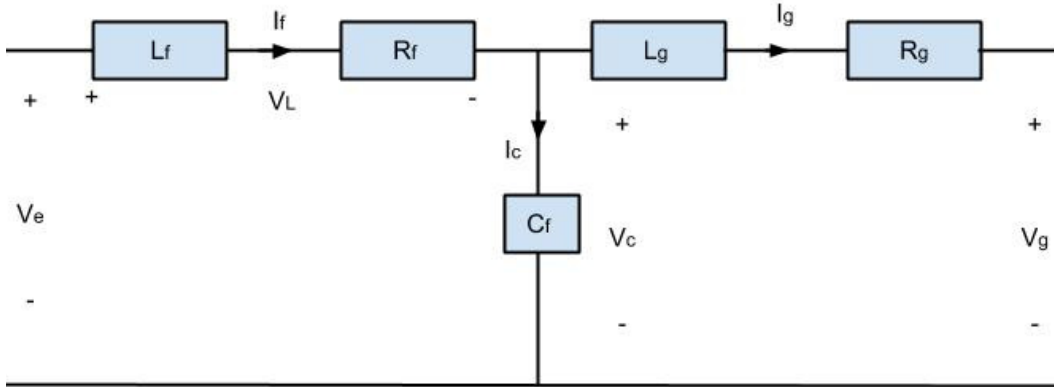
Figure 5.1: Single phase LCL filter schematic diagram

Current and voltage equation for the filter can be derived as (5-1) to (5-3) below which are valid in stationary *abc* and *αβ* reference frame [30].

$$L_f \cdot \frac{dI_f}{dt} = V_e - V_c - R_f \cdot I_f \tag{5-1}$$

$$L_g \cdot \frac{dI_g}{dt} = V_c - V_g - R_g \cdot I_g \tag{5-2}$$

$$C_f \cdot \frac{dV_c}{dt} = I_f - I_g \tag{5-3}$$

In synchronous frame, as all the voltage and current vectors are rotating with the same frequency, ω_s, the converter phase currents and voltage can be expressed in two axis synchronous dq frame. With reference of transformation equation given in (3-21) the current and voltage equations in dq-component form can be derived as in (5-4) to (5-9).

$$L_f \cdot \frac{dI_{f,d}}{dt} = V_{e,d} - V_{c,d} - R_f \cdot I_{f,d} + \omega_s \cdot L_f \cdot I_{f,q} \tag{5-4}$$

$$L_f \cdot \frac{dI_{f,q}}{dt} = V_{e,q} - V_{c,q} - R_f \cdot I_{f,q} - \omega_s \cdot L_f \cdot I_{f,d} \tag{5-5}$$

$$L_g \cdot \frac{dI_{g,d}}{dt} = V_{c,d} - V_{g,d} - R_f \cdot I_{g,d} + \omega_s \cdot L_g \cdot I_{g,q} \tag{5-6}$$

$$L_g \cdot \frac{dI_{g,q}}{dt} = V_{c,q} - V_{g,q} - R_f \cdot I_{g,q} - \omega_s \cdot L_g \cdot I_{g,d} \tag{5-7}$$

$$C_f \cdot \frac{dV_{c,d}}{dt} = I_{f,d} - I_{g,d} + \omega_s \cdot C_f \cdot V_{c,q} \tag{5-8}$$

$$C_f \cdot \frac{dV_{c,q}}{dt} = I_{f,q} - I_{g,d} - \omega_s \cdot C_f \cdot V_{c,d} \tag{5-9}$$

5.1.1   Feed Forward Compensation in Current Controller

Equations (5-4) to (5-9) above clearly show that current and voltage of d-axis and q-axis components are dependant. Simplification of the model can be done by using decoupling approach where decoupled components will be fed forward to be compensated. As feed forward approach compensate the cross coupling components, d-axis and q-axis can be controlled independently [24]. The implementation of current controller with PI controller and feed forward compensation in synchronous frame can be represented as in Figure 5.2.
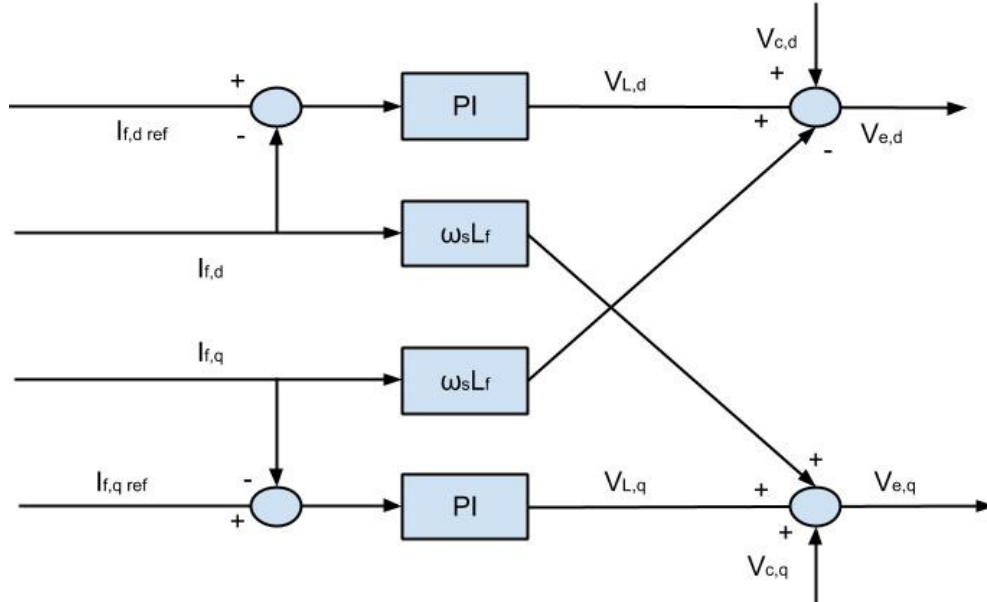
Figure 5.2: Current controller with feed forward compensation

In the current controller, with reference to (5-4) and (5-5), the feed forward compensation components $V_{cp,d}$ and $V_{cp,q}$ can be derived as in (5-10) to (5-15) below. For further simplification filter capacitor voltage is fed forward too. Since we are measuring the filter capacitor voltage thus the measured value can be used otherwise an estimation of filter capacitor voltage based on measured current can be an option.

$$V_{e,d} = L_f \cdot \frac{dI_{f,d}}{dt} + R_f \cdot I_{f,d} + V_{cp,d} \tag{5-10}$$

$$V_{e,q} = L_f \cdot \frac{dI_{f,q}}{dt} + R_f \cdot I_{f,q} + V_{cp,q} \tag{5-11}$$

$$V_{cp,d} = V_{c,d} - \omega_s \cdot L_f \cdot I_{f,q} \tag{5-12}$$

$$V_{cp,q} = V_{c,q} + \omega_s \cdot L_f \cdot I_{f,d} \tag{5-13}$$

$$V_{L,d} = L_f \cdot \frac{dI_{f,d}}{dt} + R_f \cdot I_{f,d} \qquad \text{where} \quad V_{L,d} = V_{e,d} - V_{cp,d} \tag{5-14}$$

$$V_{L,q} = L_f \cdot \frac{dI_{f,q}}{dt} + R_f \cdot I_{f,q} \qquad \text{where} \quad V_{L,q} = V_{e,q} - V_{cp,q} \qquad (5\text{-}15)$$

With the application of feed forward terms shown in (5-14) and (5-15), simplified system transfer function with Laplace transformation can be derived as in (5-16) and (5-17). Owing to their similarities, transfer function representation for both d-axis and q-axis can be expressed as (5-18) with T_f as system time constant. System transfer function is an important element in controller optimization and stability analysis which are discussed further in sections below.

$$V_{L,d}(s) = (L_f S + R_f) \cdot I_{f,d}(s) \qquad (5\text{-}16)$$

$$V_{L,q}(s) = (L_f S + R_f) \cdot I_{f,q}(s) \qquad (5\text{-}17)$$

$$L_c(s) = \frac{I_f(s)}{V_L(s)} = \frac{1}{L_f S + R_f} = \frac{1/R_f}{1 + T_f S} \qquad \text{where} \quad T_f = \frac{L_f}{R_f} \qquad (5\text{-}18)$$

Transfer function in per unit system is derived below from (5-19) to (5-24), where subscript 'b' refers to elements in base value and subscript 'pu' refers to per unit value. Basic per-unit system derivation can be found at Table 6.2.

$$V_L(s)_{pu} \cdot V_b = (L_f S + R_f) \cdot I_f(s)_{pu} \cdot I_b \qquad (5\text{-}19)$$

$$V_L(s)_{pu} = (L_f S + R_f) \cdot \frac{I_b}{V_b} \cdot I_f(s)_{pu} \qquad (5\text{-}20)$$

Where per unit inductance and resistance are defined as:

$$L_{pu} = \omega_b \cdot L \cdot \frac{I_b}{V_b} \qquad (5\text{-}21)$$

$$R_{pu} = R \cdot \frac{I_b}{V_b} \qquad (5\text{-}22)$$

$$L_c(s)_{pu} = \frac{I_f(s)_{pu}}{V_L(s)_{pu}} = \frac{1}{\left(\dfrac{L_{f,pu}}{\omega_b}\right)S + R_{f,pu}} = \frac{1/R_{f,pu}}{1 + T_{f,pu}S} \tag{5-23}$$

$$\text{where } T_{f,pu} = \frac{L_{f,pu}}{\omega_b \cdot R_{f,pu}} \tag{5-24}$$

5.1.2 Feed Forward Compensation in Voltage Controller

The same principal for feed forward compensation used in the current controller can be implemented for the voltage controller too. In voltage controller simplification process, it is assumed that there is no current flow in the grid inductance, I_g referring to Figure 5.1. This is a valid assumption because the filter is not connected to grid network during synchronization as such there will be no current flowing through grid side inductance, L_g of the filter.
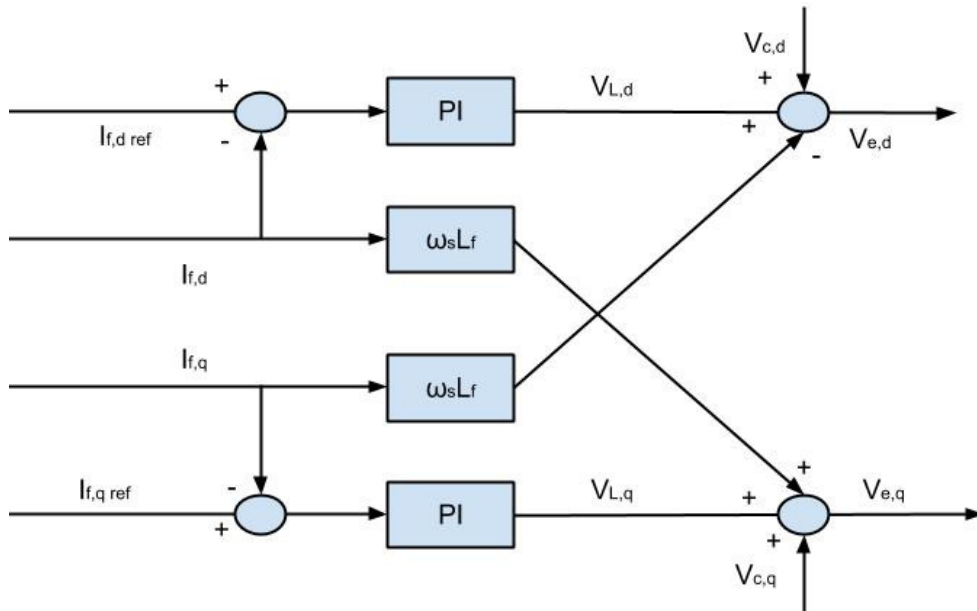
Figure 5.3: Voltage controller with feed forward compensation

Thus with reference to (5-8) and (5-9), the feed forward compensation components $I_{cp,d}$ and $I_{cp,q}$ can be derived as shown from (5-25) to (5-30) below while its graphical representation is as depicted in Figure 5.3.

$$I_{f,d} = C_f \cdot \frac{dV_{c,d}}{dt} + I_{cp,d} \tag{5-25}$$

$$I_{cp,d} = -\omega_s \cdot C_f \cdot V_{c,q} \tag{5-26}$$

$$I_{f,q} = C_f \cdot \frac{dV_{c,q}}{dt} + I_{cp,q} \tag{5-27}$$

$$I_{cp,q} = \omega_s \cdot C_f \cdot V_{c,d} \tag{5-28}$$

$$I_{L,d} = C_f \cdot \frac{dV_{c,d}}{dt} \qquad \text{where} \quad I_{L,d} = I_{f,d} - I_{cp,d} \tag{5-29}$$

$$I_{L,q} = C_f \cdot \frac{dV_{c,q}}{dt} \qquad \text{where} \quad I_{L,q} = I_{f,q} - I_{cp,q} \tag{5-30}$$

Similar to the method applied in current controller, simplified system transfer function with Laplace transformation can be derived as in (5-31) and (5-32). From their similarities, transfer function representation for both d-axis and q-axis can be written as (5-33).

$$I_{L,d}(s) = C_f S \cdot V_{c,d}(s) \tag{5-31}$$

$$I_{L,q}(s) = C_f S \cdot V_{c,q}(s) \tag{5-32}$$

$$L_v(s) = \frac{V_c(s)}{I_L(s)} = \frac{1}{C_f S} \tag{5-33}$$

Transfer function in per unit system is derived below from (5-34) to (5-36), where subscript 'b' refers to elements in base value and subscript 'pu' refers to per unit value. Basic per-unit system derivation can be found at Table 6.2.

$$I_L(s)_{pu} \cdot I_b = C_f S \cdot V_c(s)_{pu} \cdot V_b \tag{5-34}$$

Where per unit capacitance is defined as:

$$C_{pu} = \omega_b \cdot C_f \cdot \frac{V_b}{I_b} \tag{5-35}$$

$$L_v(s)_{pu} = \frac{V_c(s)_{pu}}{I_L(s)_{pu}} = \frac{\omega_b}{C_{f,pu}S}$$

<div align="right">(5-36)</div>

5.2   PI CONTROLLER OPTIMIZATION AND ANALYSIS

The discussion up to this stage would have enabled a complete control structure built as a simulation model. However for PI controller, the parameter has to be determined in order to ensure that the control system is giving the desired response. As mentioned in Chapter 3, selection of parameter for PI controller is lengthy and required knowledge of the whole system in detailed.

In this section, modulus Optimum (MO) and symmetrical optimum (SO) which were the two optimization methods presented in section 3.2 will be applied on the PI controller based control system. Approximation that was made in order to simplify and to make the calculation possible is elaborated too. Discussion follows by preliminary analysis of the system stability and dynamic performance. These parameters are applied in the simulation with its results and discussion presented in Chapter 6.

5.2.1   Inner Loop Current Controller

The current control loop can generally be represented by the block diagram as shown in Figure 5.4 below. It is a series connection of blocks representing PI controller, Converter and the filter system with a unity feedback. Each of the block diagram represent a transfer function that will be combined to form the system open loop transfer function, $G_{c,OL}(s)$ and closed loop transfer function, $G_{c,CL}(s)$ for tuning and analysis purpose.
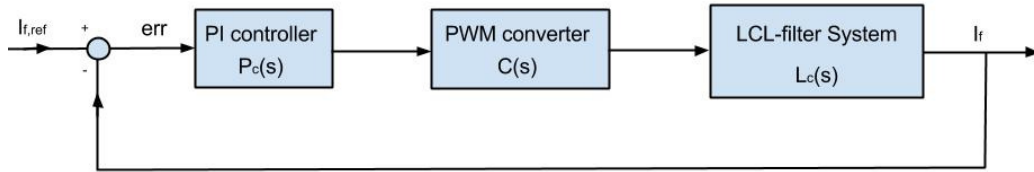
Figure 5.4: General current control block diagram with PI controller

The transfer function of PI controller block, $P_c(s)$ is given in (3-2), while converter, $C(s)$ is in (3-25) and simplified filter system in per unit system, $L_c(s)_{pu}$ in (5-23). Combining this three series connected blocks will form $G_{c,OL}(s)$ as given in (5-37) below and further derivation $G_{c,CL}(s)$ of with unity feedback is obtained as in (5-38)

$$G_{c,OL}(s) = P_c(s) \cdot C(s) \cdot L_c(s)_{pu} = K_p \cdot \left(\frac{1+T_iS}{T_iS} \right) \cdot \frac{1}{1+T_\alpha S} \cdot \frac{1/R_{f,pu}}{1+T_{f,pu}S}$$

<div align="right">(5-37)</div>

$$G_{c,CL}(s) = \frac{K_p \cdot (1+T_iS) \cdot 1/R_{f,pu}}{K_p \cdot (1+T_iS) \cdot 1/R_{f,pu} + T_iS \cdot (1+T_\alpha S) \cdot (1+T_{f,pu}S)}$$

<div align="right">(5-38)</div>

Modulus Optimum

The $G_{c,OL}(s)$ transfer function developed in (5-37) for our current control system is similar to the plant system presented in modulus optimum section 3.2.1. Both having one large time constant and one small time constant where in this system $T_{f,pu} > T_\alpha$. Thus by applying MO tuning, the controller's parameters can be defined below as well as the new system $G_{c,OL}(s)$ and $G_{c,CL}(s)$ transfer function.

$$T_i = T_{f,pu} \tag{5-39}$$

$$K_p = \frac{T_{f,pu} \cdot R_{f,pu}}{2T_\alpha} \tag{5-40}$$

$$G_{c,OL}(s) = \frac{1}{2T_\alpha S} \cdot \frac{1}{(1 + T_\alpha S)} \tag{5-41}$$

$$G_{c,CL}(s) = \frac{1/2T_\alpha^2}{S^2 + 1/T_\alpha S + 1/2T_\alpha^2} \tag{5-42}$$

In order to analyse the stability of the system, two quantitative measures defined as gain margin (GM) and phase margin (PM) can be used. The greater of these two quantities indicates the system greater ability to withstand changes in system parameters before become unstable. GM and PM can be determined for the system open loop bode diagram. More detailed information on GM and PM can be found in Appendix A.

Referring to converter system's parameter used in this thesis, as tabulated in Table 6.3, parameter's of PI controller can be found as $T_i = 3.8$ and $K_p = 1.4383$ and subsequently the $G_{c,OL}(s)$ can be found as below. Figure 5.5 is the open loop transfer function bode diagram of the control system, it can be seen that PM can be approximated to be 66° which is within acceptable margin and GM is at approximately 69.7dB, indicating a stable and non-oscillating response to step input. For satisfactory dynamic response without oscillations, PM should be greater than 45°, preferably close to 60° while GM should be more than 3dB [27]. It is observed that the crossover frequency, f_c is noted to be at 7330 rad/s (1167 Hz), which is close to seven times lower than converter switching frequency, f_{sw}. f_c is usually chosen to be one or two times smaller than f_{sw} to avoid interference from switching frequency noise [39]. Figure 5.6 shows the step response in time domain.

$$G_{c,OL}(s) = \frac{1.2829e^8}{(S^2 + 1.6018e^4 S)} \tag{5-43}$$
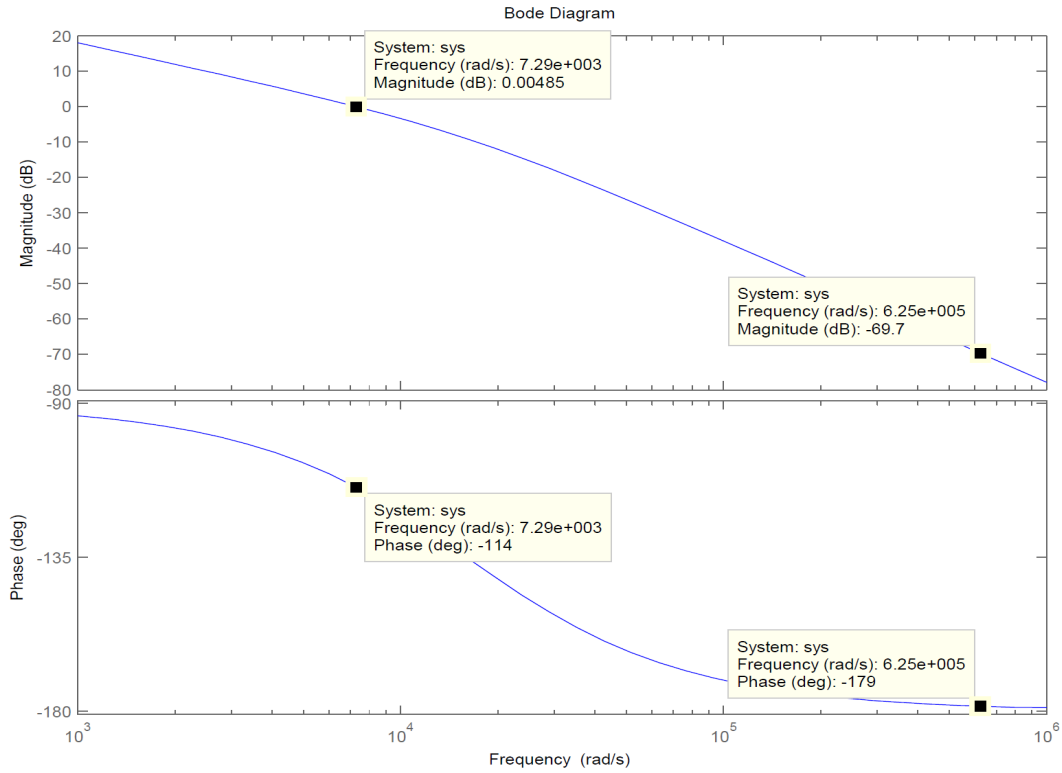
49

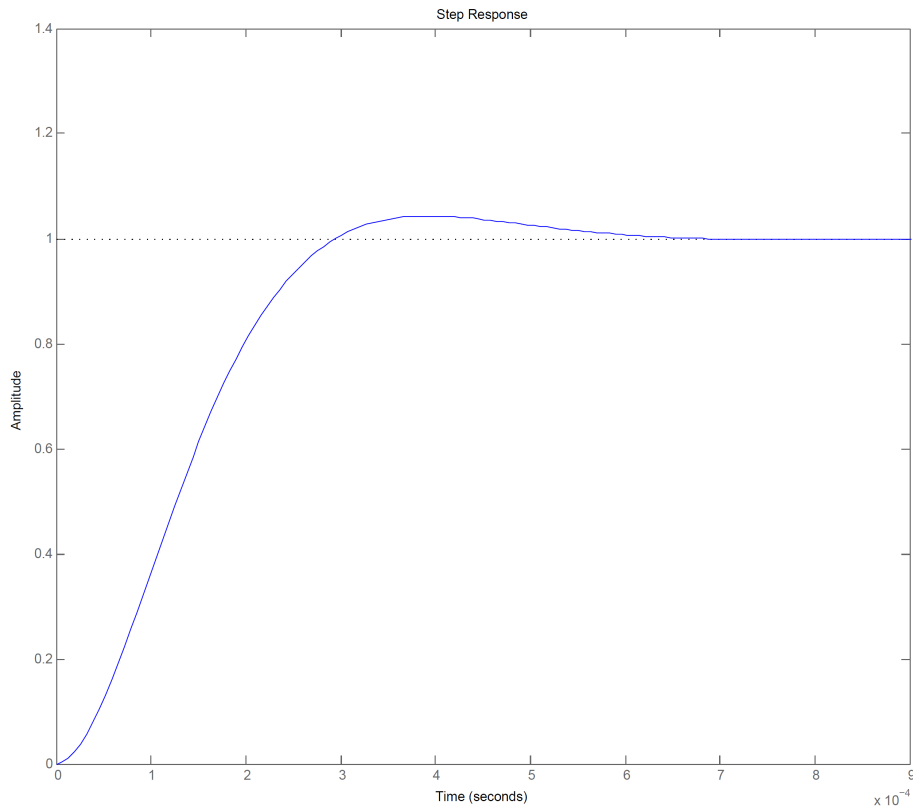Figure 5.5: Open loop bode diagram for current controller with MO

Figure 5.6: Step response for current controller with MO

Symmetrical Optimum

Referring to the $G_{c,OL}(s)$ in (5-37) and the same converter's parameter used as in MO, optimization with SO tuning can be carried out with reference to (3-15) and (3-16) as presented in section 3.2.2. With $T_{f,pu} > T_\alpha$, controller's parameter and the corresponding $G_{c,OL}(s)$ general form can be expressed as below.

$$T_i = \sigma^2 \cdot T_\alpha \tag{5-44}$$

$$K_p = \frac{T_{f,pu} \cdot R_{f,pu}}{\sigma \cdot T_\alpha} \tag{5-45}$$

$$G_{c,OL}(s) = \frac{T_{f,pu}}{\sigma^3 \cdot T_\alpha^2 S} \cdot \frac{\left(1 + \sigma^2 \cdot T_\alpha S\right)}{\left(1 + T_\alpha S\right)\left(1 + T_{f,pu} S\right)} \tag{5-46}$$

The conventional SO tuning is with setting of $\sigma = 2$ while the recommended range by [40] is between 2 to 4. Thus the analysis here will include three selected value by using $\sigma = 2$, $\sigma = 3$ and $\sigma = 4$ for comparison purpose. After a lengthy mathematical derivation the controller's parameters and its open loop transfer function can be found as below:

For ($\sigma = 2$), $T_i = 2.4972e^{-4}$ and $K_p = 1.4383$

$$G_{c,OL}(s) = \frac{1.2829e^8 S + 5.1372e^{11}}{S^3 + 1.6018e^4 S^2 + 4.2152e^3 S} \tag{5-47}$$

For ($\sigma = 3$), $T_i = 5.6187e^{-4}$ and $K_p = 0.9589$

$$G_{c,OL}(s) = \frac{8.5525e^7 S + 1.5221e^{11}}{S^3 + 1.6018e^4 S^2 + 4.2152e^3 S} \tag{5-48}$$

For ($\sigma = 4$), $T_i = 9.9888e^{-4}$ and $K_p = 0.7192$

$$G_{c,OL}(s) = \frac{6.4144e^7 S + 6.4216e^{10}}{S^3 + 1.6018e^4 S^2 + 4.2152e^3 S} \tag{5-49}$$

Figure 5.7 shows open loop bode diagram for current controller with SO tuning for the three chosen value of σ. All lines in the diagram indicate a system with good GM and f_c where the highest is approximately six times lower than f_{sw} which is vital to avoid switching noise interference. However it can be seen for conventional tuning ($\sigma = 2$), PM of the transfer function is merely 37° which is significantly lower than recommended value (PM > 45°) for a satisfactory dynamic response without oscillation. Nevertheless, it appears that as σ increases PM will increase which indicate a trend toward a more robust

system though a decreasing f_c means slower system response. The compromising effect is obviously shown where as robustness of the system increases the response will be slower. This is significantly indicated in Figure 5.8 which depicts the step response in time domain.
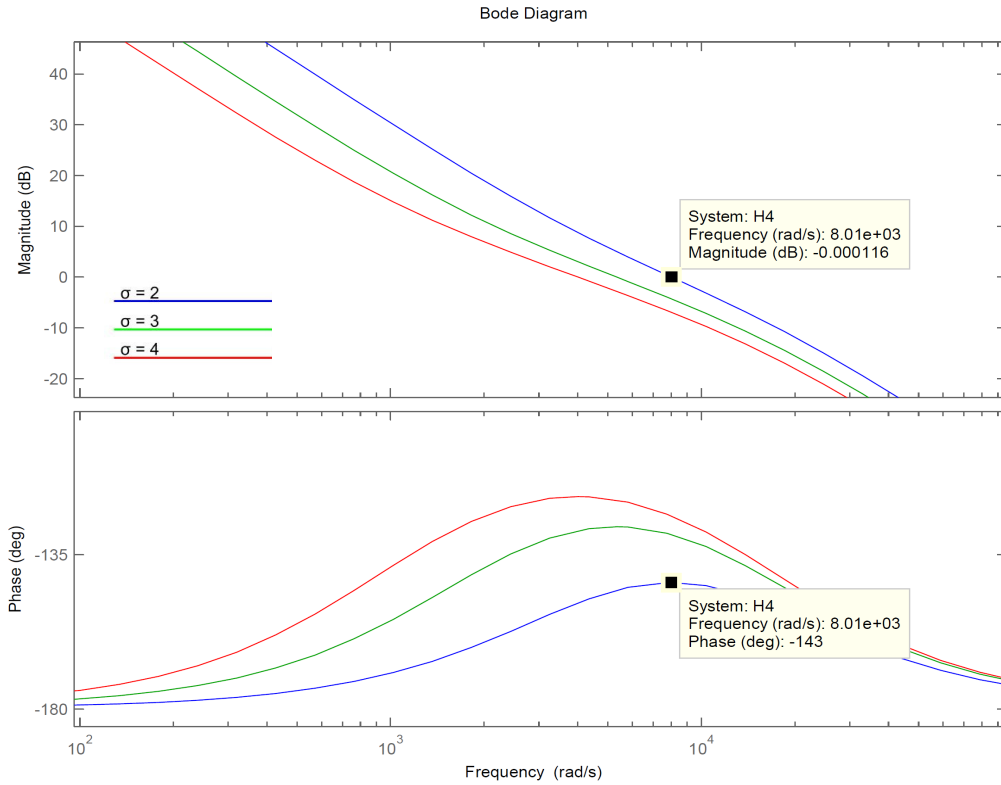

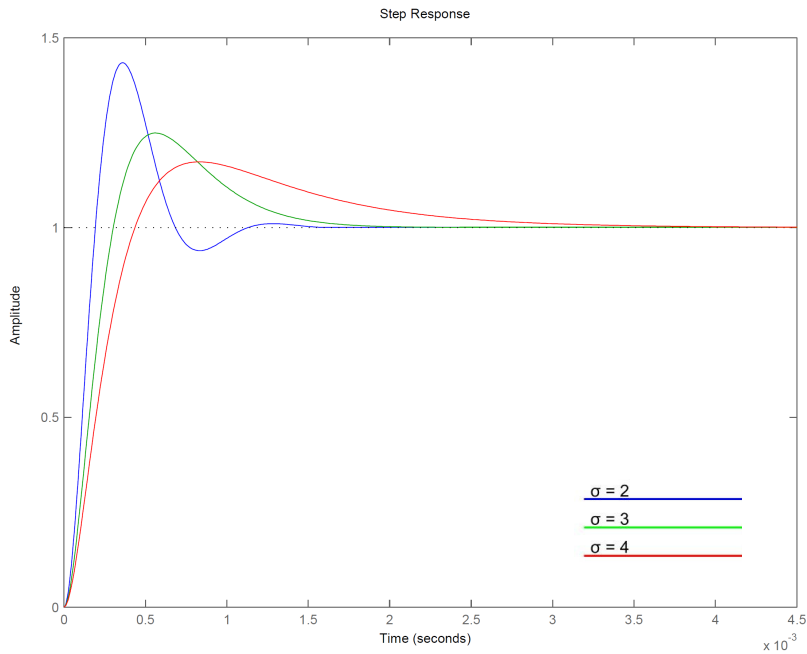Figure 5.7: Open loop bode diagram for current controller with SO

Figure 5.8: Step response for current controller with SO

5.2.2 Outer Loop Voltage Controller

Outer voltage control loop can be illustrated as in Figure 5.9 consist of a series connection of voltage PI controller, inner current control loop and filter system with a unity feedback. A similar approach used in current control loop shall be applied here to express the voltage control open loop, $G_{v,OL}(s)$ and closed loop, $G_{v,CL}(s)$ transfer function before proceeding with optimization tuning and stability analysis.
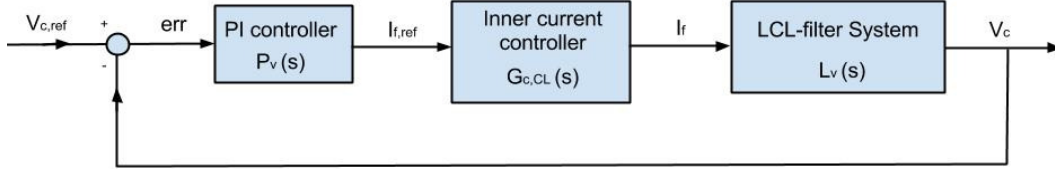
Figure 5.9: General voltage control block diagram with PI controller

The voltage PI controller transfer function, $P_v(s)$ is the general transfer function for PI controller as expressed in (3-5) while simplified filter system transfer function for voltage controller in per unit, $L_v(s)_{pu}$ can be derived as in (5-36).

First Order Approximation

The inner current control closed loop transfer function, $G_{c,CL}(s)$ after MO tuning is initially found to be as in (5-42) which is a second order transfer function. $G_{c,CL}(s)$ tuned with SO is not discussed here due to its complexity. Referring to table in Appendix B, optimization tuning with a PI controller is not possible in a combination of an integrator found in $L_v(s)_{pu}$ with a second order transfer function, $G_{c,CL}(s)$. Thus a first order approximation of $G_{c,CL}(s)$ is derived as a simplification approach for voltage controller tuning purpose. [30]

(5-42) together with second order function general expression (3-14) can be expressed in another form as shown in (5-50) and (5-51)

$$G_{c,CL}(s) = \frac{1}{2T_\alpha^2 S^2 + 2T_\alpha S + 1} \tag{5-50}$$

$$G_{CL}(s) = \frac{1}{\frac{1}{\omega_o^2}S^2 + \frac{2\zeta}{\omega_o}S + 1} \tag{5-51}$$

For frequency lower than ω_o, $1/\omega_o^2 \ll 1$ and thus first order approximated function can be derived as (5-52)

$$G_{c,CL}(s) = \frac{1}{\frac{2\zeta}{\omega_o}S + 1} = \frac{1}{2T_\alpha S + 1} \tag{5-52}$$

Putting all the blocks transfer function in series together, (3-5), (5-36) and (5-52) the new first order approximation, voltage control open loop, $G_{v,OL}(s)$ and closed loop, $G_{v,CL}(s)$ transfer function can be found as:

$$G_{v,OL}(s) = P_v(s) \cdot G_{c,CL}(s) \cdot L_v(s)_{pu} = K_p \cdot \left(\frac{1 + T_i S}{T_i S} \right) \cdot \frac{1}{1 + 2T_\alpha S} \cdot \frac{\omega_b}{C_{f,pu} S} \qquad (5\text{-}53)$$

$$G_{v,CL}(s) = \frac{K_p \cdot (1 + T_i S) \cdot \omega_b}{K_p \cdot (1 + T_i S) \cdot \omega_b + T_i S \cdot (1 + 2T_\alpha S) \cdot (C_{f,pu} S)} \qquad (5\text{-}54)$$

In Figure 5.10 below, current control second order closed loop transfer function (5-50) and its first order approximation (5-52) are depicted on the same bode diagram for comparison. It is significant to note their similarity for frequency lower than ω_o.

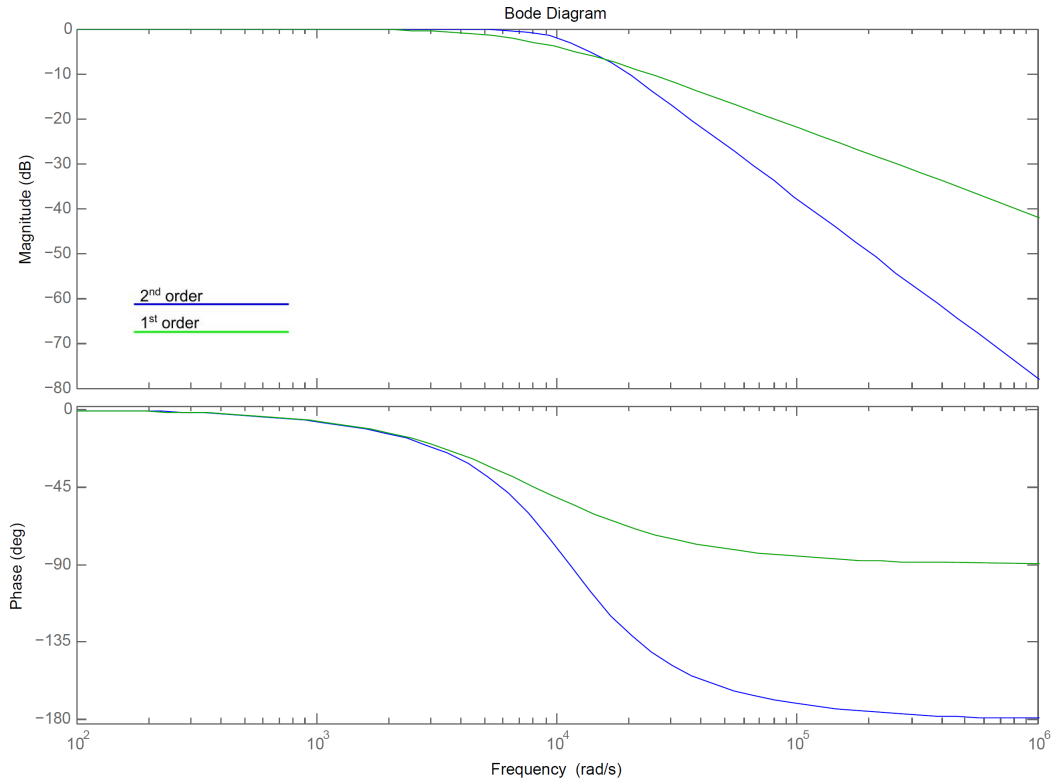Figure 5.10: Bode diagram of first order approximation and second order current control closed loop transfer function

Symmetrical Optimum

With reference to voltage control open loop transfer function (5-53) and SO tuning rules for one integrator and one time constant as presented in (3-18) and (3-19), parameter for PI controller and the corresponding $G_{v,OL}(s)$ can be expressed as below.

$$T_i = \sigma^2 \cdot 2T_\alpha \qquad\qquad (5\text{-}55)$$

$$K_p = \frac{C_{f,pu}}{\sigma \cdot T_\alpha \cdot \omega_b} \qquad\qquad (5\text{-}56)$$

$$G_{v,OL}(s) = \frac{\left(1 + \sigma^2 \cdot 2T_\alpha S\right)}{\left(4\sigma^3 T_\alpha^{\,2} S^2\right) \cdot \left(1 + 2T_\alpha S\right)} \qquad\qquad (5\text{-}57)$$

With the same approach as in current controller, parameter σ with value of 2, 3 and 4 is selected for stability and step response analysis. With these selections, a trend or differences between the σ values can be seen easily. A tedious mathematical task gives the results of controller parameter and the transfer function as below.

For (σ = 2), $T_i = 4.9944e^{-4}$ and $K_p = 2.1185$

$$G_{c,OL}(s) = \frac{3.2072e^7 S + 6.4216e^{10}}{S^3 + 8.009e^3 S^2} \qquad\qquad (5\text{-}58)$$

For (σ = 3), $T_i = 1.1237e^{-3}$ and $K_p = 1.4123$

$$G_{c,OL}(s) = \frac{2.1381e^7 S + 1.9027e^{10}}{S^3 + 8.009e^3 S^2} \qquad\qquad (5\text{-}59)$$

For (σ = 4), $T_i = 1.9978e^{-3}$ and $K_p = 1.0595$

$$G_{c,OL}(s) = \frac{1.6036e^7 S + 8.0269e^9}{S^3 + 8.009e^3 S^2} \qquad\qquad (5\text{-}60)$$

In Figure 5.11, open loop bode diagram for voltage controller with SO tuning for all three selected value for σ are shown. As can be seen all the σ gives good GM and f_c where the highest is approximately twelve times lower than f_{sw}. Except for (σ = 2) where its PM is deemed to be in an unstable region for satisfactory dynamic response without oscillation which can be found in Figure 5.12. Nevertheless, it appears that as σ increases PM will increase which indicate a trend toward a more stabile system though a decreasing f_c which means slower system response. This is the compromising effect of system robustness and the system response speed in tuning the PI controller.
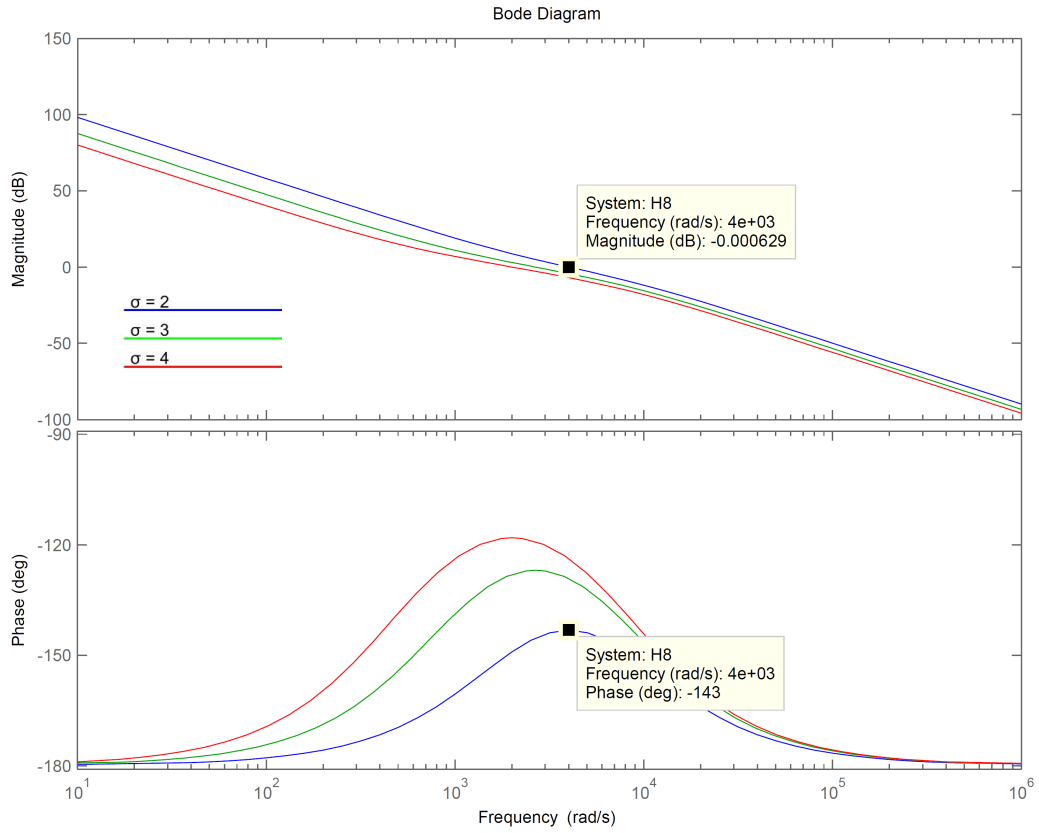
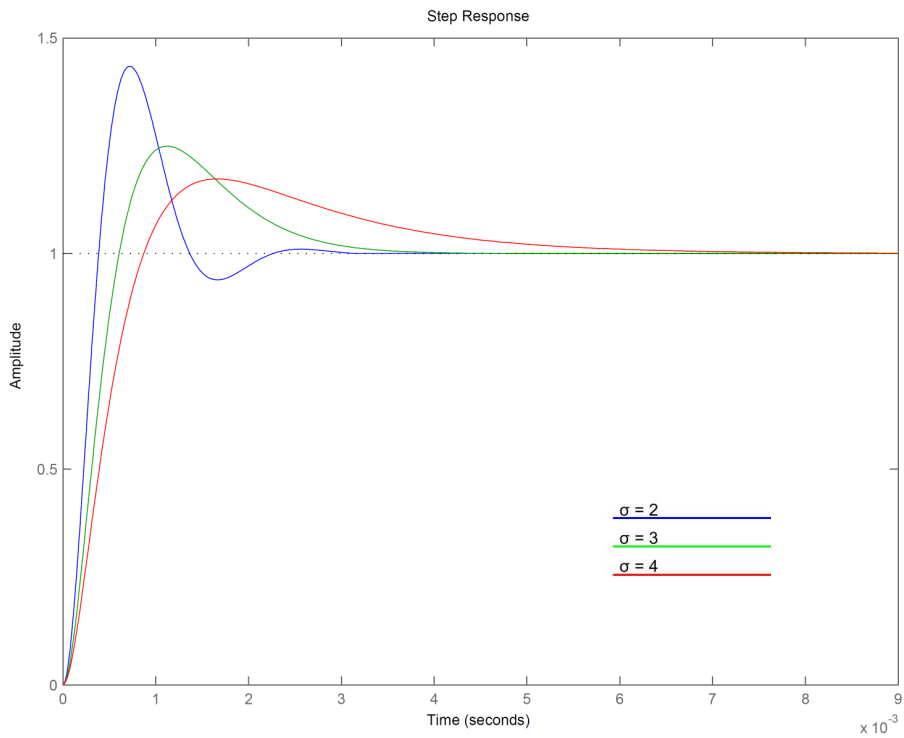Figure 5.11: Open loop bode diagram for voltage controller with SO

Figure 5.12: Step response for voltage controller with SO

6 SIMULATION RESULTS AND DISCUSSIONS

This chapter starts with introduction of the simulation programme, converters rating and parameter together with the synchronizing criteria implemented in the simulation work. Simulation results and discussion are divided into two parts, starting with current controller and followed by voltage controller utilizing the converter design which was discussed in previous chapters. It is important to note that all simulation results shown in this chapter are the best results obtained after final experimental fine tuning based on designed parameters.

6.1 COMPLETE CONVERTER SIMULATION MODEL

The active converter simulation model in this thesis is build with Simulink®, developed by MathWorks Inc. which is a ubiquitous tool for modelling and simulation. It utilized SimPowerSystems™ library which has component libraries and analysis tools for modelling and simulating electric power system. Further details about this library and Simulink can be found on the MathWorks webpage link:

http://www.mathworks.se/products/simpower/

The entire base concept and components of the model is developed by Wärtsilä, Norway. Due to right of ownership by Wärtsilä, the active converter model in Simulink is classified as a confidential file. Principal drawings of simulation model can be referred at Appendix C which will be limited from publishing.

All simulation works that were carried out in the project is run by this single integrated active converter model. Minimal modification has been made in order to implement several different control philosophies which were thoroughly discussed in Chapter 3, 4 and 5. With courtesy of Wärtsilä, the main block diagram of the converter model is as depicted in Figure 6.1 below.
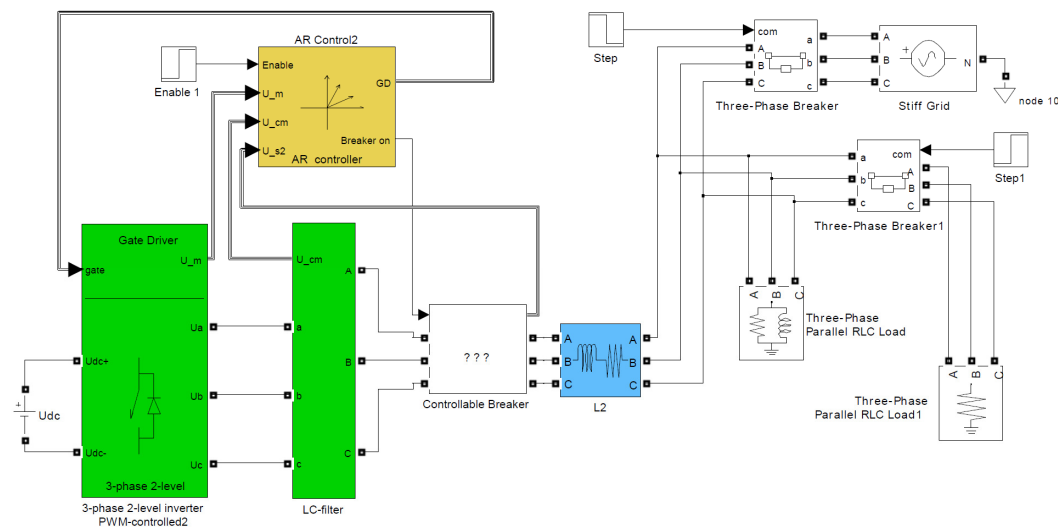
Figure 6.1: Simulink model of grid connected active converter (diagram courtesy of Wärtsilä)

This project is utilizing the converter and LCL filter parameters based on Tore Skjellnes doctoral thesis [53]. The main reason for choosing these parameters is due to the possibility for future implementation on hardware based system which is available in Norwegian University of Science and Technology laboratory. However, the implementation on hardware based system is not covered in the scope of this thesis. Table below shows the system rated parameters and filter parameters in physical and per unit value.

Table 6.1: Converter unit system ratings

Parameter	Symbol	Quantity
Rated line voltage	$V_{n, rms}$	230 V_{rms}
Nominal frequency	f_n	50 Hz
Rated current	$I_{n, rms}$	12.551 A_{RMS}
PWM switching frequency	f_{sw}	8009 Hz
DC voltage	V_{dc}	450 V

Table 6.2: Converter unit per unit system

Parameter	Symbol	Quantity
Base voltage (peak phase voltage)	$V_b = \sqrt{\dfrac{2}{3}} V_{n,rms}$	187.79 V
Base current	$I_b = \sqrt{2} I_{n,rms}$	17.75 A
Base angular frequency	$\omega_b = 2\pi f_n$	314.159 rad/s
Base impedance	$Z_b = \dfrac{V_n}{I_n}$	10.58 Ω
Base inductance	$L_b = \dfrac{Zb}{\omega_b}$	33.677 mH
Base capacitance	$C_b = \dfrac{1}{Z_b \omega_b}$	300.86 μF

Table 6.3: LCL filter parameters

Parameter	Symbol	Quantity	Per Unit	Quantity
Converter side filter inductance	L_f	1.95 mH	$L_{f,pu}$	0.05642
Converter side filter resistance	R_f	0.5 mΩ	$R_{f,pu}$	47.26e^{-6}
Filter capacitance	C_f	50 μF	$C_{f,pu}$	0.1662
Grid side filter inductance	L_g	1.35 mH	$L_{g,pu}$	0.04009

| Grid side filter resistance | R_g | 3.5 mΩ | $R_{g,pu}$ | $32.72e^{-6}$ |

Table 6.4: Criteria for grid synchronization (close breaker)

Parameter	**Error limit**
Voltage magnitude error	0.1 pu
Voltage frequency error	0.02 pu
Voltage phase angle error	4°
Breaker closing time setting (in voltage control)	0.1 s

6.2 CURRENT CONTROLLER

The objective of the simulation results presented in this section is to identify and discuss the differences between various current control strategies implementation. There are three subsections below presenting three different approaches with the application of PI controller in synchronous *dq* and stationary *αβ* frame and hysteresis controller in stationary *abc* frame.

Although optimization tuning for PI controller was carried out in Chapter 5 to determine its parameter, it is the eventual experimental fine tuning that give the best results which are shown here. It is important to note that the measured signal here in current control system is the filter current, I_f and the current reference is a step input required to obtain 1pu of capacitor voltage. This is considered to be the worst case scenario for current controller during synchronization.

6.2.1 PI Controller in Synchronous *dq* Frame

The current control in synchronous *dq* frame is found to give best control response by using SO tuning with σ = 2.5, giving $T_i = 3.9e^{-4}$ and $K_p = 1.7979$. However a better control response is found by tuning the PI controller gain lower to $K_p = 0.7$. First window in Figure 6.2 below shows results of dq-axis reference and actual current where red and blue line is for d-axis reference and actual current respectively and purple and green line for q-axis reference and actual current respectively. While in the second window converter three phase actual current is plotted.

An input of 0.1662pu for q-axis current is the required current for voltage capacitor to be 1pu as to match with grid reference voltage which can be calculated as below. Thus a step input of 0.1662pu is considered to be the worst case scenario in the current controller during synchronization. Simulation is set with a step input at 0.01s, results shows that it takes around 0.015 seconds for both axes current to be stable with fixed switching frequency due to PWM observed on the three phase actual current.

$$I_c = V_b \cdot 2\pi f C_f = 2.9498A \qquad (6\text{-}1)$$

$$I_{pu} = \frac{I_c}{I_b} = 0.1662 \, pu \tag{6-2}$$

Changes in d-axis reference current while a step input is imposed on q-axis suggest a non-perfect decoupling. A heavy oscillation during initial step input is due to charging of filter capacitor voltage from 0pu to 1pu and the limitation set to the maximum allowed output of PI controller in order to protect the converter from over current. The later constant oscillation is likely to be filter resonance effect. This setting will serve as the current control model for voltage control loop design.
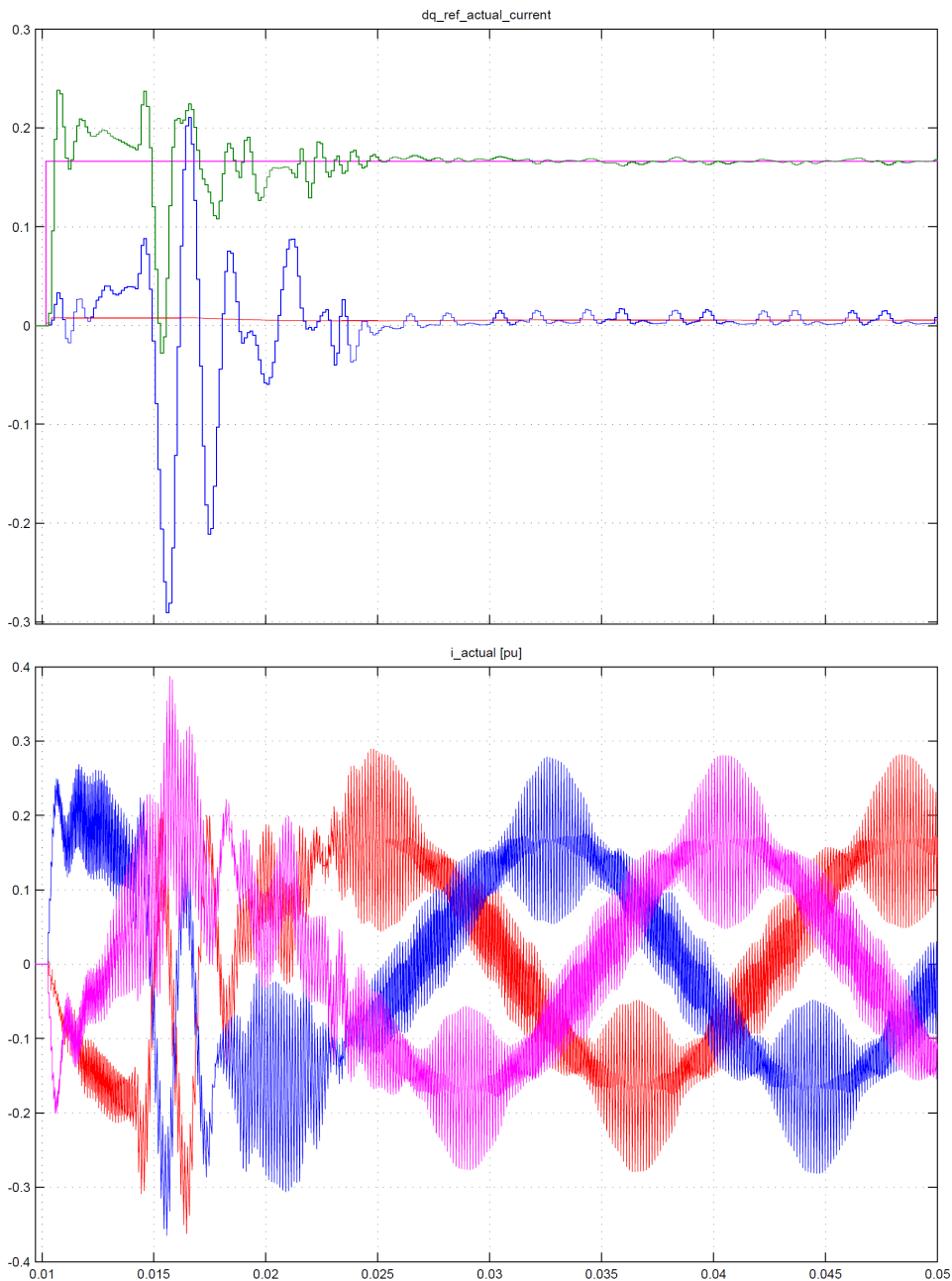

Figure 6.2: dq-axis current response to step input of 0.1662pu.

6.2.2 PI Controller in Stationary *αβ* Frame

In simulating current controller model in stationary αβ frame, same parameter for PI controller as above is applied which is $K_p = 0.7$ and $T_i = 3.9e^{-4}$. Results is presented in Figure 6.3 below where the first window shows αβ-axis reference and actual current where red and blue line is for α-axis reference and actual current respectively and purple and green line for β-axis reference and actual current respectively. The second window shows converter three phase actual current.

A step input of 0.1662pu is given at 0.01s for β-axis current and the result shows a constant sinusoidal current error with approximately 0.15pu peak to peak. It is significant to notice that in stationary αβ frame, PI controller is working in correction of a sinusoidal error signal. It is proven that PI controller works much better in a DC error signal as discussed in section 6.2.1. This constant current error simply means that filter capacitor is not able to achieve 1pu voltage as required. It can be observed through the peak value of three phase actual current in second window which is about 0.1pu. This is significantly lower than the required 0.1662pu input reference. Constant switching frequency is noted on the three phase current with the implementation of PWM.

<u>Feed Forward Compensation</u>

Although theoretically suggests that decoupling components is not relevant in stationary αβ frame structure, an experimental simulation with feed forward compensation of decoupling components similarly implemented in section 6.2.1 synchronous *dq* frame is carried out for investigation.

The results are captured in Figure 6.4, apparently result indicates with feed forward compensation the current controller manage to lower the error despite heavier oscillation, with one of the reason due to the current limiting set on the PI controller. In general the three phase actual current produces the required magnitude despite being more distorted in comparison with three phase actual current shown in Figure 6.2. It will be premature to have a conclusion now on this implementation, further study is necessary to support this result.
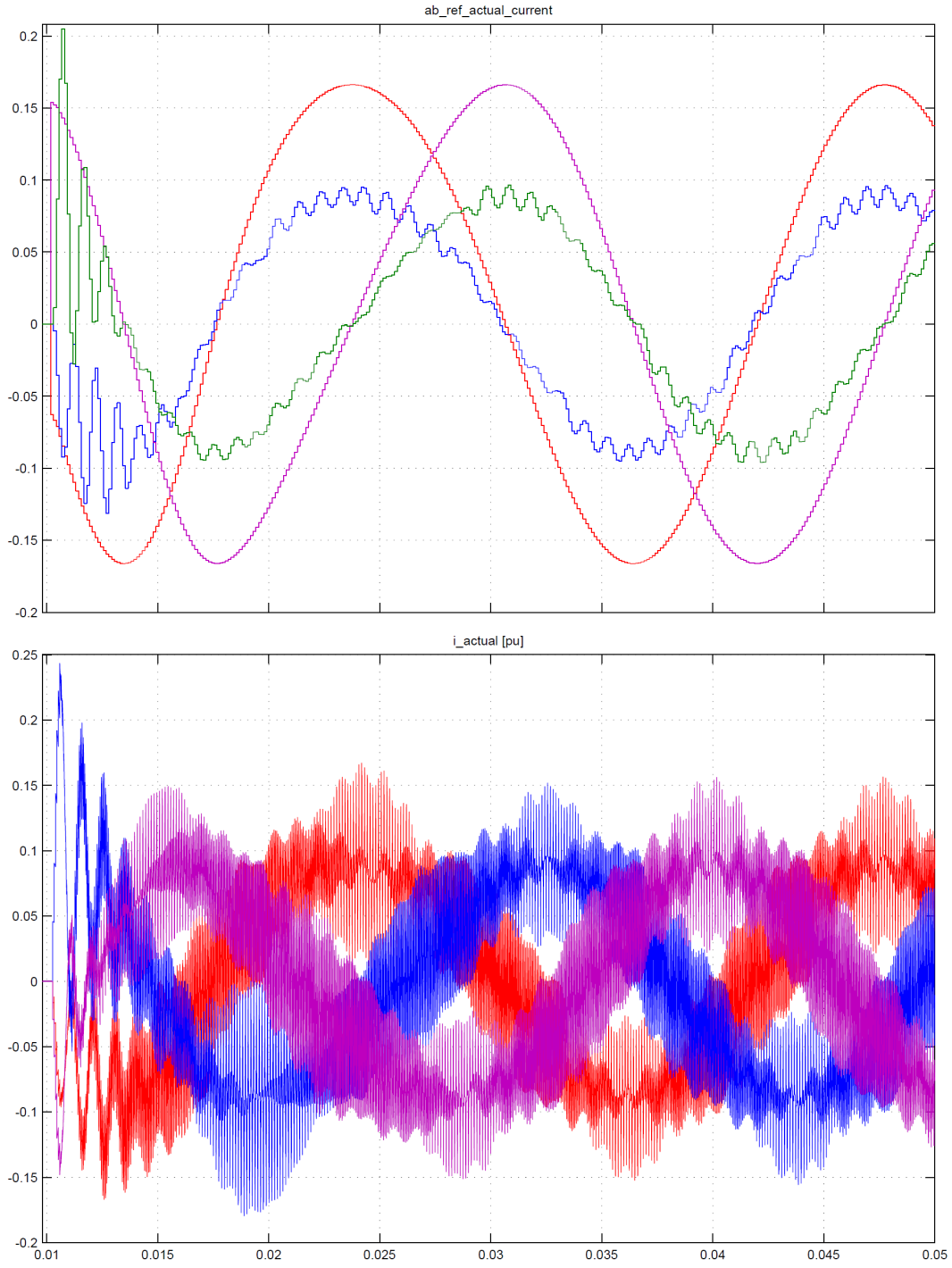
Figure 6.3: αβ-axis current response to step input of 0.1662pu
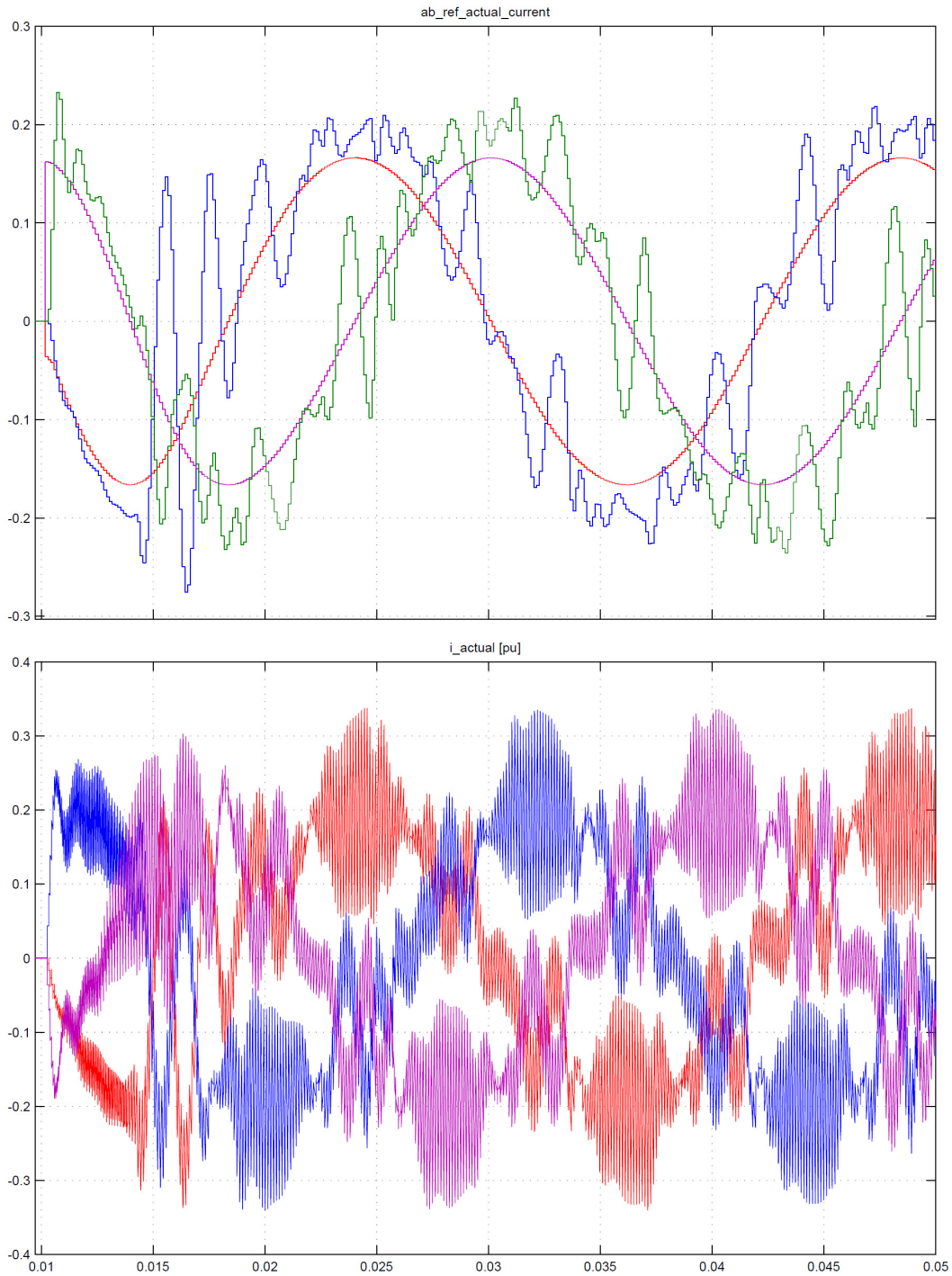
Figure 6.4: αβ-axis current response to step input of 0.1662pu (with feed forward compensation)

6.2.3   Hysteresis Controller in Stationary *abc* Frame

Hysteresis controller in stationary *abc* frame is a simple and direct control method. Unlike PI controller the only parameter required to be set for hysteresis controller is the tolerance band. By using the same converter model as before a step input of 0.1662 pu is given at 0.01s to simulate the worst case scenario in this converter control system during

synchronization. Simulation results of different tolerance band are presented below for comparison.

Figure 6.5 shows the actual three phase current with tolerance band set as 0.09pu which is approximately 54.15% of the current input value. Simulation results in the same order are plotted on Figure 6.6 and Figure 6.7 with tolerance band of 0.02pu (12.03%) and 0.16pu (96.27%) respectively.

From the plots for various tolerance band, it can be inferred that hysteresis controller generally has a fast and accurate control response, however its accuracy are dependant on the tolerance bandwidth setting. Higher tolerance band width results in lower control accuracy and switching frequency which will generally result in a higher harmonic current waveform and subsequently affecting the filter capacitor voltage waveform albeit not vividly seen in the simulation results here. On the other hand, lower tolerance band width gives higher accuracy for current control and switching frequency simultaneously in general. Thus a compromising effect between control accuracy and switching frequency in hysteresis control has to be taken into consideration in designing hysteresis controller.

Regardless of bandwidth setting, hysteresis controller does produce an irregular switching frequency. The irregularity is dependant on input source voltage level, load system parameters and tolerance bandwidth setting. This in effect generates a more complex harmonics in current waveform and will be a challenge in the design for harmonic filtering.
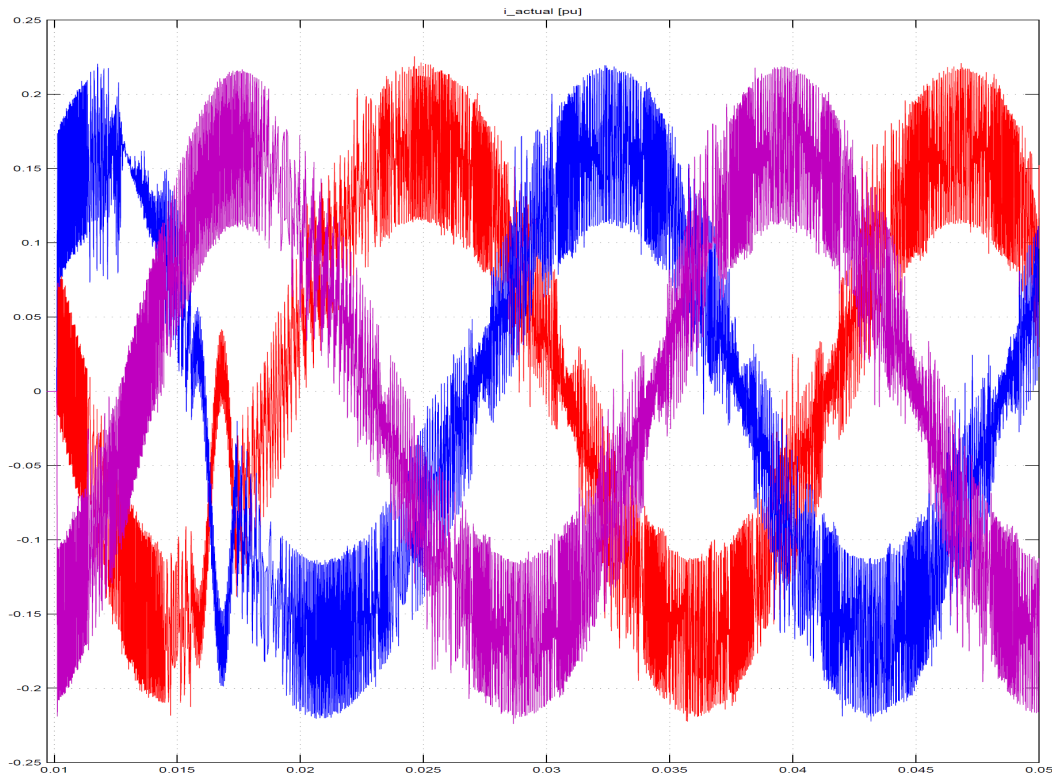

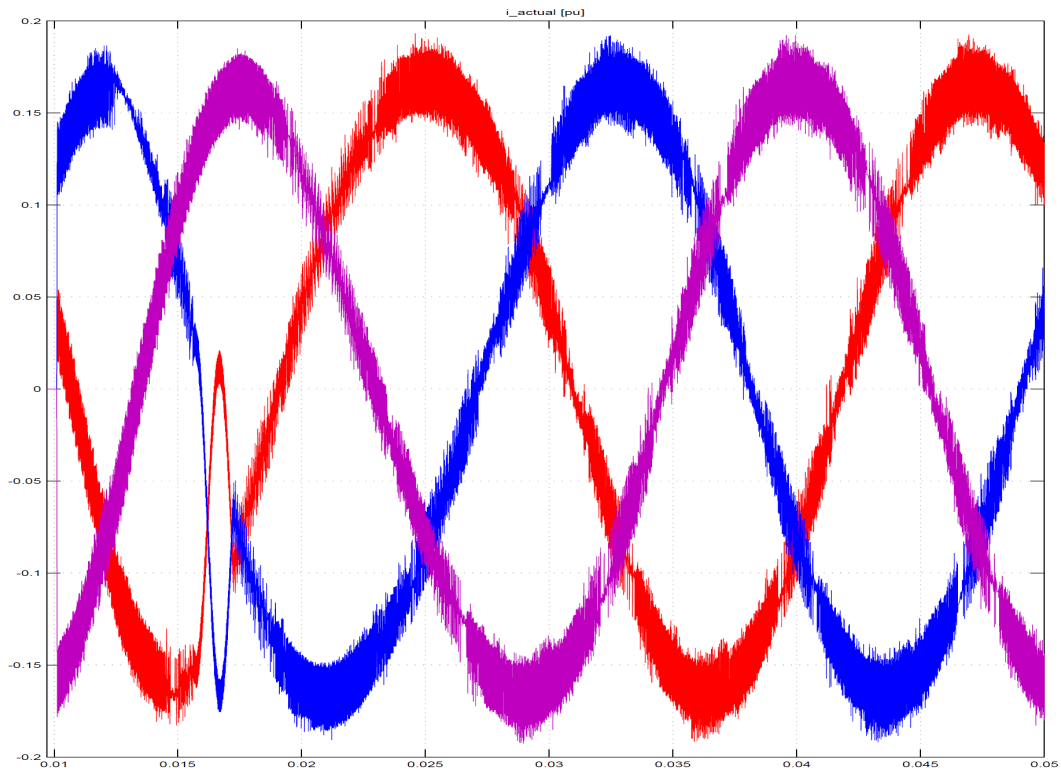Figure 6.5: Hysteresis current control with tolerance band of 0.09pu

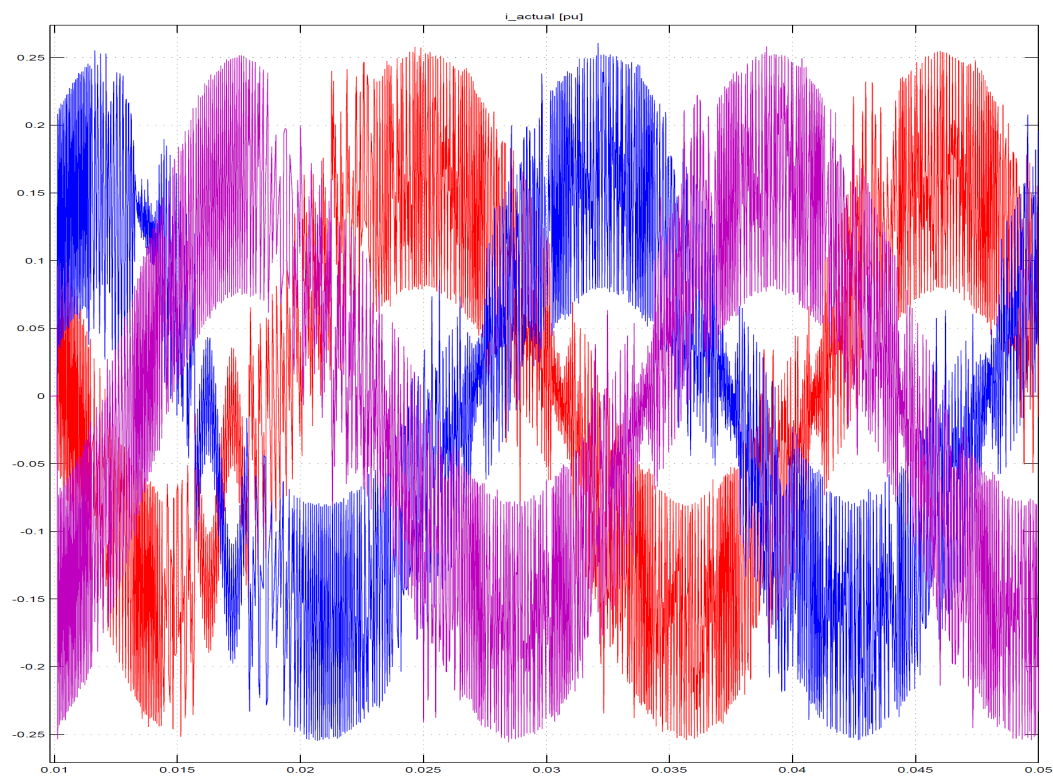Figure 6.6: Hysteresis current control with tolerance band of 0.02pu

Figure 6.7: Hysteresis current control with tolerance band of 0.16pu

6.3   VOLTAGE CONTROLLER

The voltage control simulation results is implemented with three different control methodologies, namely application of PI controller in synchronous *dq*, stationary *αβ* frame and the magnitude and frequency-phase angle control in synchronous *dq* frame. Each of the approach is presented in subsections below.

It is important to note that the reference voltage here is the grid voltage, V_g and the measured voltage is filter capacitor voltage, V_c as defined before. Refer to Figure 4.1 for clear pictorial representation of these signals. The current controller model used in voltage control loop is a common model for all approach which can be referred at section 6.2.1. In voltage control system simulation, grid breaker ready to close signal is set at 0.1s. Upon matching the grid synchronization criteria the breaker will close and the transient response is observed.

6.3.1   PI Controller in Synchronous *dq* Frame

Voltage control in synchronous *dq* frame is responding well to SO tuning with σ = 3 as presented in section 5.2.2 which give value of $T_i = 1.12e^{-4}$ and $K_p = 1.41$. Nevertheless a fine tuning with $K_p = 0.5$ gives best simulation results as shown in Figure 6.8 below. The first window shows results of dq-axis reference and actual voltage where red and blue line represents d-axis reference and actual current respectively and purple and green line for q-axis reference and actual current respectively. The second window gives the three phase filter capacitor voltage waveform, V_c.

At 0.01s, PI controller starts to match V_c with the reference grid voltage, V_g which is consistently at 1pu, thus this serve as a voltage step input of 1pu at 0.01s. The start up of the system with zero charge filter capacitor is recognised as the worst case scenario in grid synchronization. Simulation results indicate heavy oscillation and a surge of error during start up and it takes about 0.015 seconds for both axes voltage to be stable. The voltage control response is rather fast considering the time taken for inner current controller to become stable is approximately 0.015 seconds too as discussed in section 6.2.1.

Prior to closing of grid synchronization, control in synchronous frame gives a zero steady state error despite small oscillation which could be due to noise interference and filter resonance effect. It is vital to notice in a cascaded control structure, a robust inner current control is inevitable for a good outer voltage control performance. The second window shows a smooth three phase filter capacitor voltage at 1pu in steady state.

Grid breaker was observed closing at 0.1s and the transient response is significantly noticeable. Upon closing of grid breaker, the control should switch from grid synchronization control to normal operation controls which will in turn controlling the voltage reference input based on desired active and reactive power delivered. However, due to the absence of normal operation control this transient response is prolonged and deemed to be worst transient expected.
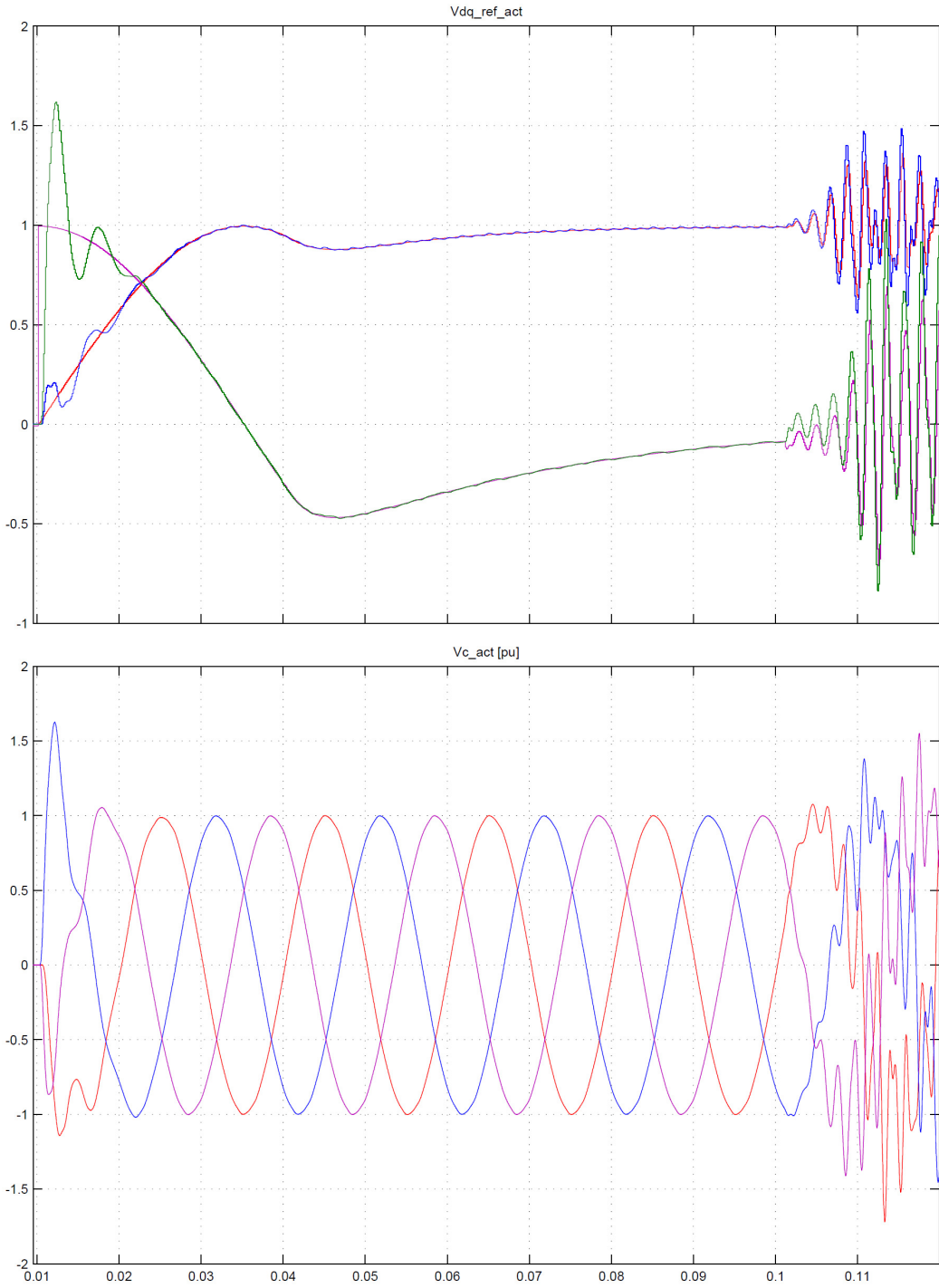
Figure 6.8: dq-axis voltage response to system start up

6.3.2   PI Controller in Stationary *αβ* Frame

For simulation of voltage controller in stationary αβ frame, same parameter for PI controller and model for inner current control loop as in section 6.3.1 is implemented. The only change lies on the voltage control reference frame in order to have a distinct comparison for PI voltage controller working in different reference frame. Simulation results is as depicted in Figure 6.9, where the first window shows results of αβ-axis reference and actual voltage where red and blue line represents α-axis reference and actual voltage respectively and purple and green line for β-axis reference and actual voltage respectively. Second window is plotting the three phase filter capacitor voltage waveform, V_c.

With PI controller initialized to match V_c with the reference grid voltage, V_g at 0.01s, a surge and heavy oscillation during start up is noticeable. Similarly this characteristic appears in synchronous frame control too and considered to be the worst case scenario in grid synchronization. In terms of time taken for voltage waveform to stabilize is rather identical to synchronous frame where it takes about 0.015 seconds, thus the voltage control speed is said to be equally fast.

However as expected in stationary frame control a steady state sinusoidal voltage error approximated at 0.3pu peak to peak is clearly visible. This is due to PI controller inability to correct a sinusoidal error signal while it works perfectly in correcting DC error signal. Results also shows that filter capacitor voltage, V_c is not able to be controlled at 1pu as required due to the steady state error.

Grid breaker was observed closing at 0.1s and the transient response is clearly visible. After closing of grid breaker, control should switch from grid synchronization control to normal operation control which will in turn controlling the voltage reference input based on desired active and reactive power delivered. However, due to the absence of normal operation control this transient response is prolonged and deemed to be worst transient expected.

Feed Forward Compensation

Theoretically, decoupling components is not relevant in stationary αβ frame structure but an experimental simulation with feed forward compensation of decoupling components implemented in synchronous frame as in section 6.3.1 is carried out for investigation. Results are shown in Figure 6.10 in the same order as Figure 6.9. It is vividly seen that the steady state sinusoidal voltage error has been eliminated. The good control of voltage αβ-axis voltage translates into a well controlled V_c too as shown in the three phase voltage waveform with the peak of 1pu as required which is similar to voltage control response as in synchronous frame given in Figure 6.8. Further investigation is needed to be carried out in order to make a conclusion on this implementation.
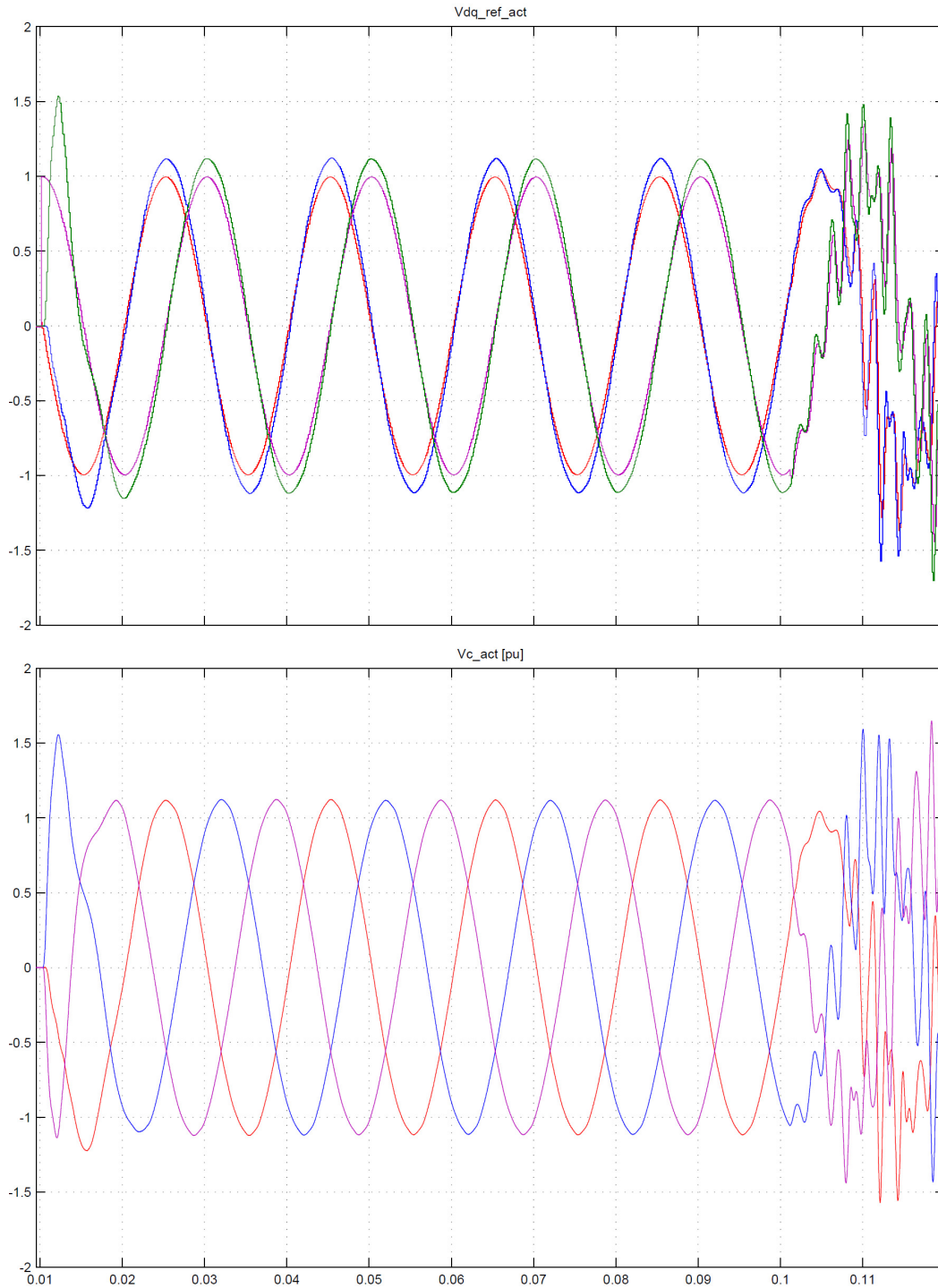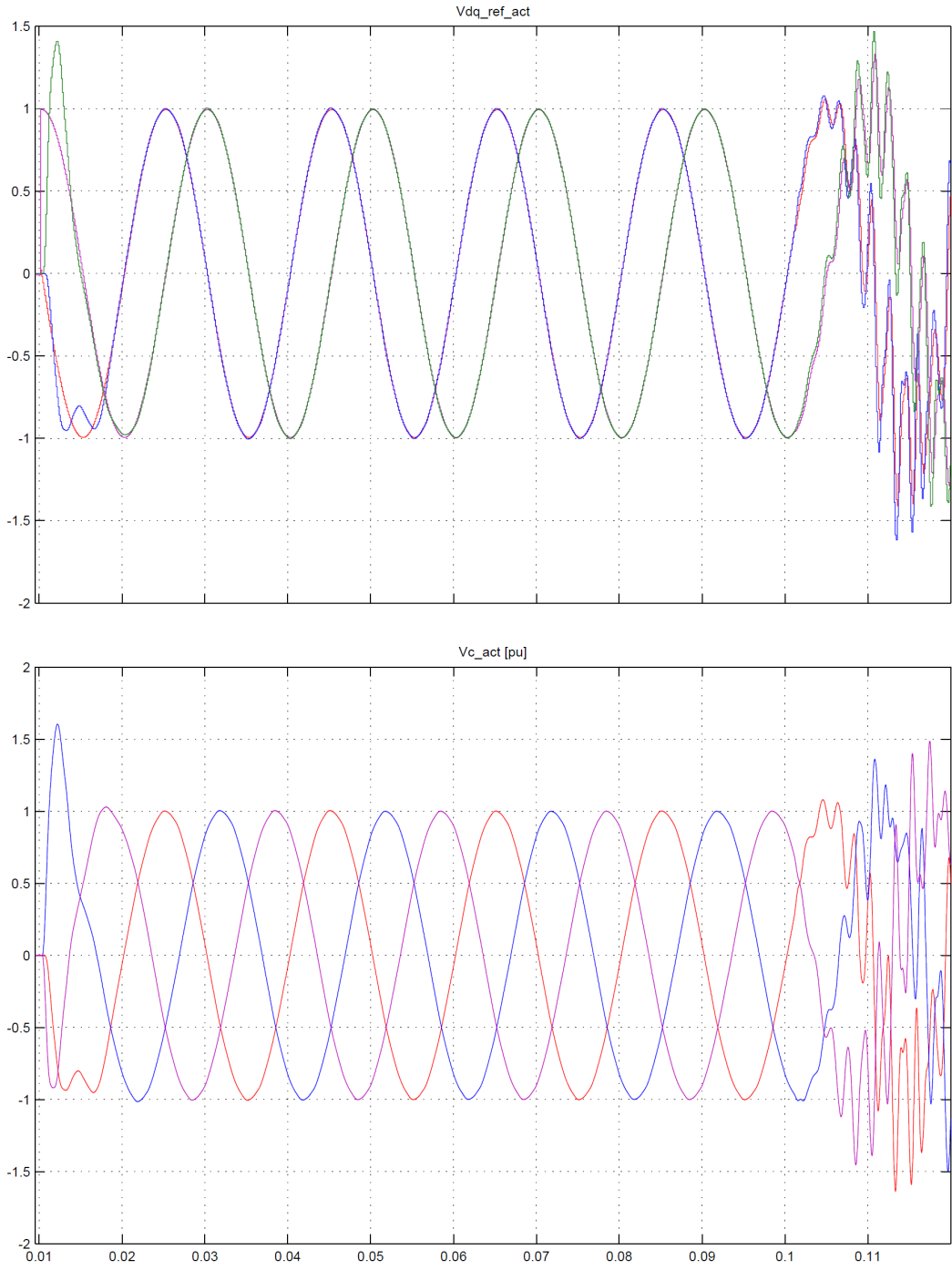
Figure 6.9: αβ-axis voltage response to system start up

Figure 6.10: αβ-axis voltage response to system start up (with feed forward compensation)

6.3.3 Magnitude and Frequency-Phase Angle PI Controller in Synchronous *dq* Frame

In this approach, voltage will be controlled separately in synchronous dq reference frame as presented in section 4.3.3. Voltage magnitude error will be corrected by the q-axis PI controller while frequency and phase angle error by the d-axis PI controller. The controllers parameter setting are purely by experimental tuning and found to work best with $T_i = 0.01$ and $K_p = 0.15$ for d-axis PI controller and $T_i = 0.05$ and $K_p = 0.8$ for q-axis PI controller. Figure 6.11 depicts the simulation results with the first three windows showing the voltage components error in order of frequency, phase angle and magnitude while the last windows plots the three phase filter capacitor voltage, V_c.

q-axis PI controller for voltage magnitude error is set to start operation at 0.01s similar to all other simulation before while d-axis is being prohibited to start until 0.05s. Both d and q axis are theoretically dependant on each other in the formation of three phase sinusoidal voltage signal. However the principal of this approach where the control of both axes are independant unlike in section 6.3.1 and section 6.3.2 results in lower limitation for error tolerance. As such in this application magnitude of V_c is filtered and given a start value of 0.9pu for synchronization. Which literally means a charged up filter capacitor during initialization. Similar approach can be applied on voltage control structure before to minimize the start up oscillation.

PI controller for voltage frequency and phase angle error in d-axis, is given a delay to start at 0.05s. The reason for this delay is to avoid the controller from attempting to correct a highly unstable frequency measurement during the initialization period. With this delay unnecessary surge of current is avoided. The control algorithm here allows frequency error which act as input to the PI controller to be corrected with phase angle control interuption. Once phase angle error is detected beyond the limit set, phase angle controller will inject a pseudo error into the controller input attempting to bring the phase angle error into the limit by manipulating the frequency of V_c. The pseudo error is set as 0.05pu for angle error larger than 4º for this simulation and 0.005pu for angle error between 2º and 4º. No pseudo error will be injected for angle error less than 2º. The time delay and limit setting on the controller is highly flexible and can be adjusted independantly to suit the need of different model.

Results in Figure 6.11 below indicates all voltage components error manage to achieve the criteria of closing breaker for grid synchronization with minimum oscillation within 0.15s. A smooth three phase V_c waveform at 1pu matching the grid reference votlage is observed too. The main advantage of this control lies in its independance and flexibility of control.

Grid breaker was observed closing at 0.16s and the transient response is observed. Upon closing of grid breaker, the control should switch from grid synchronization control to normal operation control which will in turn controlling the voltage reference input based on desired active and reactive power delivered. However, due to the absence of normal operation control this transient response is prolonged and deemed to be worst transient expected.
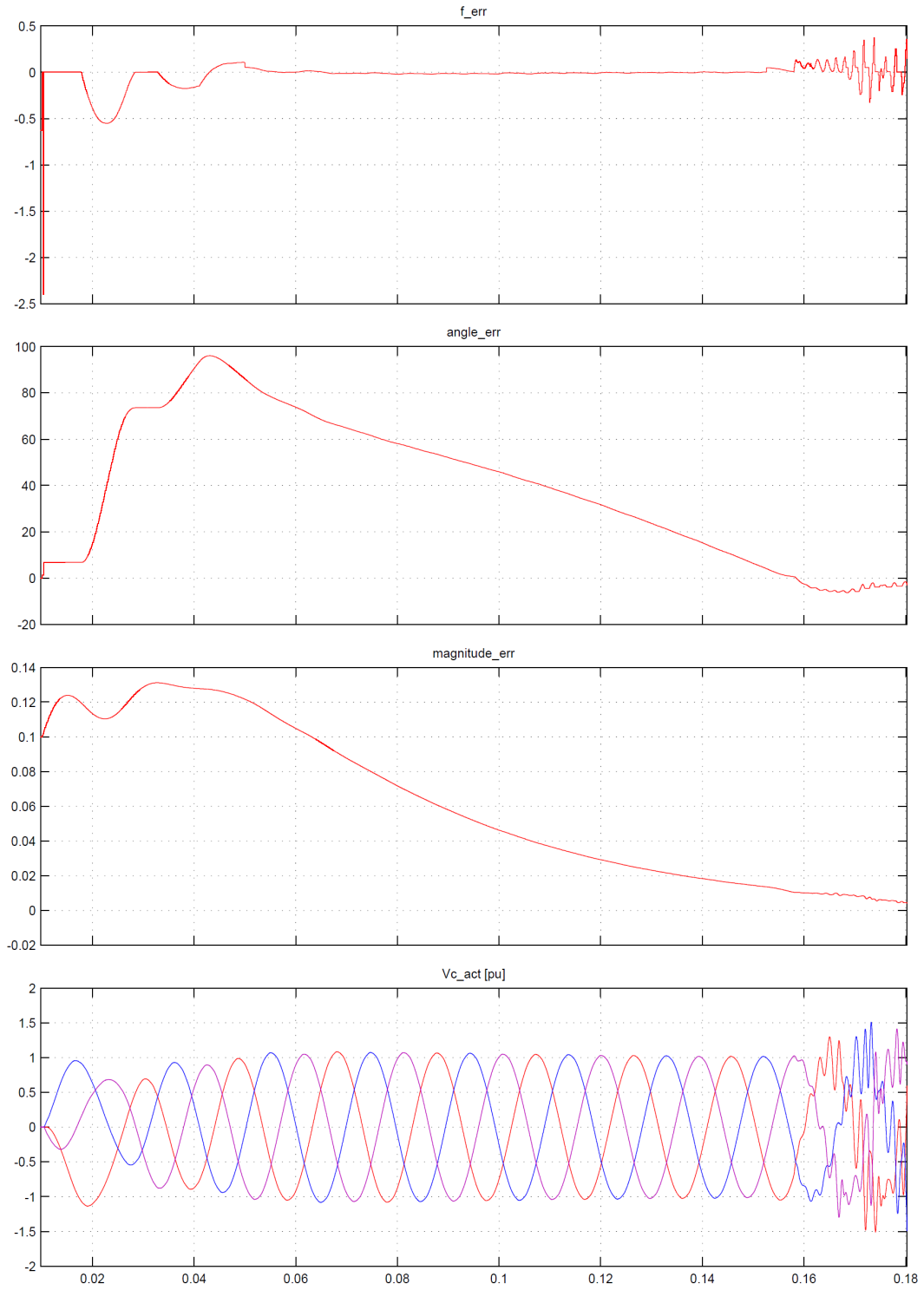
Figure 6.11: Voltage components error and three phase V_c waveform

7   CONCLUSION AND PROPOSAL FOR FUTURE RESEARCH

This chapter is divided into two sections with first section concludes the most important aspect of this thesis. While the second section proposes ideas for work that can be done in future research either within this thesis scope for improvised findings or out of this thesis scope for potential control strategy to be investigated.

7.1   CONCLUSION

In this thesis, current and voltage control strategy for grid synchronization in a cascaded converter control structure have been modelled and simulated with Simulink. Each of the control strategy has been tested with three different control approaches with results and discussion presented in Chapter 6. Based on these, conclusion can be made as below.

Current Control

Current control with PI controller found to be working better in synchronous *dq* reference frame compare to stationary *αβ* reference frame. As in synchronous frame, PI controller is correcting DC error signal instead of an AC error signal which will lead to a steady state sinusoidal error. This simply means the controlled current will not match the input reference current.

By implementing feed forward compensation of coupling components in stationary *αβ* frame as applied in *dq* synchronous frame, the steady state error seems to be minimizing despite a more distorted three phase filter current observed. The effect of this implementation requires further investigation for a solid conclusion.

While for hysteresis controller in three phase stationary *abc* reference frame, three phase filter current waveform is observed to be responding generally fast and accurately controlled within the tolerance band. However its accuracy is dependant on the tolerance bandwidth setting. Hysteresis controller approach is much simpler than PI controller approach as the knowledge of the system and load parameter is not needed in designing the controller. Nevertheless control in three phase reference frame requires three identical controllers compare to two controllers in two phase reference frame.

Hysteresis controller produces an irregular switching frequency while PI controller with PWM gives a fixed converter switching frequency. The irregularity is dependant on input source voltage level, load system parameters and tolerance bandwidth setting. This in effect generates a more complex harmonics in current waveform and will be a challenge in the design for harmonic filtering.

Voltage Control

Voltage control with PI controller in synchronous *dq* reference frame and stationary *αβ* reference frame in general share the same observation as in current control. Thus it can be similarly concluded where control in synchronous frame is found to be a better option as it will not lead to steady state error. Despite the steady state error, both control approaches are able to achieve the grid synchronizing criteria and seen connected to grid

at 0.1s. Grid breaker ready to close signal is set to at 0.1s. Upon closing of grid breaker, the transient response is vividly visible. Due to the absence of normal operation control this transient response is prolonged and deemed to be worst transient expected.

Similar experiment was carried out by implementing feed forward compensation of coupling elements in stationary frame and results shown was optimistic with almost zero steady state error and producing smooth and accurate three phase filter voltage as obtained in synchronous frame. Further theoretical study is needed to support the result obtained.

Previous implementation was aimed to simulate the worst case scenario with a 1pu step input during initialization and zero charged filter capacitor. However in voltage magnitude and frequency-phase angle controller where both axes are controlled separately, the system has lower tolerance for step input during initialization. Thus capacitor was pre charged to 0.9pu which effectively simulating a step input of 0.1pu. This similar approach can be applied to previous voltage control strategies to reduce the oscillation during system initialization.

Results showns all voltage components error manage to achieve the criteria of closing breaker for grid synchronization with minimum oscillation within 0.15s. A smooth three phase V_c waveform at 1pu matching the grid reference votlage is observed too. Although this control structure has a lower tolerance in input error and slower in syncrhonizing, the main advantage of this control lies in its independance and flexibility of control. Where the voltage and frequency reference can be given independantly without the need of generating sinusoidal voltage reference.

7.2 PROPOSAL FOR FUTURE RESEARCH

Apart from the limited methods that have been presented here due to time and resource limitation, some scope that deemed to be fit for future research have been recognised progressively during this project and thus proposed as below:

Within Thesis Scope for Improvement
- Active and passive damping approach for harmonic compensation
- Theoretical study for parameter design of voltage magnitude and frequency PI controller
- Sophisticated design phase-angle controller
- Feed forward compensation in stationary $\alpha\beta$ reference frame

Out of Thesis Scope for Potential Research
- Implementation of proportional resonant controller
- Development of normal operation control system
- Comparison of power quality of various strategies

8   REFERENCES

[1]   Dan Krotz, "Microgrids: reliable power in a small package," (www.lbl.gov/Science-Articles/Archive/EETD-microgrids.html), February 2003

[2]   J. Martin, "Distributed vs centralized electricity generation: are we witnessing a change of paradigm," HEC Paris, May 2009

[3]   J. A. Momoh, S. Meliopoulus, R. Saint, "Centralized and distributed generated power system – a comparison approach," PSERC publications 12-08, June 2012

[4]   "Kyoto protocol to the United Nations framework convention on climate change," United Nations, 1998

[5]   Denzil Merrill, "Central vs distributed power infrastructure," (http://ecmweb.com/content/central-vs-distributed-power-infrastructure), December 2005

[6]   Zpryme Research and Consulting, "Power systems of the future: the case for energy storage, distributed generation and microgrids," November 2012

[7]   R. H. Lasseter, "Microgrid: a conceptual solution," PESC 04, June 2004

[8]   P. Dondi, D. Bayoumi, C. Haederli, D. Julian, M. Suter, "Network integration of distributed power generation," Journal of power sources 106 (2002) 1-9

[9]   M. Bollen, F. Hassan, "Integration of distributed generation in the power system," John wiley & sons, 2011

[10]   E. F. Camacho, T. Samad, M. G. Sanz, I. Hiskens, "Control for renewable energy and smart grids," IEEE css, 2011

[11]   A. Timbus, "Grid monitoring and advanced control of distributed power generation systems," Phd. Aalborg University, May 2007

[12]   U.S department of energy, "Smart grid," (energy.gov/oe/technology-development/smart-grid)

[13]   Galvin Electricity Initiative, "What are smart microgrids," (galvinpower.org/microgrids)

[14]   Electric Power Research Institute, "Integrating smart distributed energy resources with distribution management systems," September 2012

[15]   S. M. Amin, B. F. Wollenberg, "Toward a smart grid," IEEE power & energy magazine, September/October 2005

[16]   M. S. Jimenez, "Smart grid mandate: standardization mandate to European Standardisation Organisations to support European smart grid deployement," European Commission, March 2011

[17]   S. F. Bush, "Communications for the smart grid," IEEE, September 2011

[18]   S. F. Bush, "Smartgrid – communication – enabled intelligence for the electric power grid," John wiley & sons, 2013

[19]   J. M. Guerrero, "Microgrids: connecting renewable energy sources into the smart grid," EPE 11, September 2011

[20]   Siemens microgrids web page, (http://w3.siemens.com/smartgrid/global/de/produkte-systeme-loesungen/grid-applications/microgrids/pages/default.aspx)

[21]   "IEEE1547-2003: Standard for interconnecting distributed resources with electric power systems," IEEE, 2003

[22]   S. Heier, "Grid integration of wind energy conversion systems," John wiley & sons, 2006

[23]   T. Ackermann, "Wind power in power systems," John wiley & sons, 2012

[24]   C. Bajracharya, "Control of VSC-HVDC for wind power," NTNU, June 2008

[25]   F. Blaabjerg, Z. Chen, S. B. Kjaer, "Power electronics as efficient interface in dispersed power generation systems," IEEE, September 2004

[26]   F. Blaabjerg, R. Teodorescu, M. Liserre, A. V. Timbus, "Overview of control and grid synchronization for distributed power generation," IEEE, October 2006

[27]   N. Mohan, "Electrical drives and integrated approach," MNPERE, 2001

[28]   A. Perera, "Virtual synchronous machines-based power control in active rectifiers for microgrids," NTNU, July 2012

[29]   J. lettl, J. Bauer, L. Linhart, "Comparison of different filter types for grid connected inverter," PIERS, March 2011

[30]   S. E. Evju, "Fundamentals of grid connected photo voltaic power electronic converter design," NTNU, June 2007

[31]   M. Liserre, F. Blaabjerg, S. Hansen, "Design and control of an LCL filter based three phase active rectifier," IEEE, October 2005

[32]   T. C. Y. Wang, Z. Ye, G. Sinha, X. Yuan, "Output filter desing for a grid interconnected three phase inverter," IEEE, 2003

[33]   M. H. Bierhoff, F. W. Fuchs, "Active damping for three phase PWM rectifiers with high order lien side filters," IEEE, February 2009

[34]   R. Teodorescu, M. Liserre, P. Rodriguez, "Grid converters for photovoltaic and wind power systems," John wiley & sons, 2011

[35]   N. Mohan, T. M. Undeland, W. P. Robbins, "Power electronics: converters, applications and design," John wiley & sons, 2003

[36]   Fujitsu Semiconductor Limited, "PI regulator," July 2011

[37]   K. Astrom, T. hagglund, "PID controllers: theory, design and tuning," ISA, 1995

[38]   J. Suul, M. Molinas, L. Norum, T. Undeland, "Tuning of control loops for grid connected voltage source converters," IEEE, December 2008

[39]   C. Bajracharya, M. Molinas, J. A. Suul, T. M. Undeland, "Understanding of tuning techniques of converter controllers for VSC-HVDC," IEEE, June 2008

[40]   M. Machaba, M. Braae, "Explicit damping factor specification in symmetrical optimum tuning of PI controllers," AFCON, December 2003

[41]   O. Aydin, A. Akdag, P. Stefanuitti, N. Hugo, "Optimum controller design for a multilevel AC-DC converter system," IEEE, 2005

[42]   S. Preitl, R. E. Precup, "An extension of tuning relations after symmetrical optimum method for PI and PID contollers," Automatica 35 (1999) 1731-1736, April 1999

[43]   J. W. Umland, M. Safiuddin, "Magnitude and symmetric optimum criterion for the design of linear control systems: what is t and how does it compare with the others?," IEEE, June 1990

[44]   Texas Instruments, "Clarke and park transforms on the TMS320C2xx," Application report, Literature number: BPRA048, 1997

[45]   H. A. Toliyat, S. G. Campbell, "DSP based eletromechanical motion control," CRC press, 2004

[46]   D. G. Holmes, T. A. Lipo, "Pulse width modulation for power converters: principles and practice," IEEE press, 2003

[47]   J. C. Ulvin, "Grid integration of the wave energy converter bolt2," NTNU, June 2012

[48]   M. Liserre, "Modulation and current/voltage control of the grid converter," lecture slides

[49]   D. G. Holmes, T. A. Lipo, B. P. Mcgrath, W. Y. Kong, "Optimized design of stationary frame three phase AC current regulators," IEEE, November 2009

[50]   A. Maswood, "A PWM voltage source inverter with PI controller for instantaneous motor current control," IEEE, 1995

[51]   J. Hwang, M. Winkelnkemper, P. W. Lehn, "Design of an optimal stationary frame controller for grid connect AC-DC converters," IEEE, 2006

[52]   G. William, "Modeling, analysis and control of active front end (AFE) converter," Phd. NTNU, October 2007

[53]   S. Tore, "Digital control of grid connected converters for distributed power generation," Phd NTNU, March 2008

[54]   Mathworks documentation center, http://www.mathworks.se/help/control/ref/margin. html

APPENDIX A: CONTROL THEORY

A simplified control system representation as in Figure A.1, consists of a system plant and controller with Laplace domain transfer function represented as $G_p(s)$ and $G_c(s)$. Output of the system $X(s)$ is feedback in unity and compared with the reference input $X^*(s)$. The error will be corrected by the controller to achieve ideally zero error when output equals to input. The design of controller is mean to achieve criteria listed below [27]:

- Zero steady state error
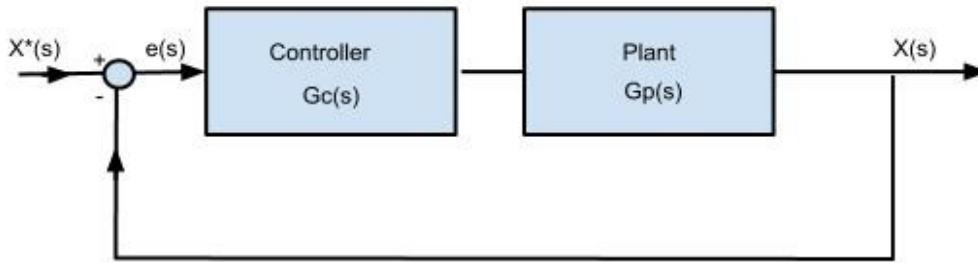- Good dynamic response (fast transient response)

Figure A.1: Generic block diagram for a unity feedback control system

In order to ensure above criteria are met, the open loop transfer function, $G_{OL}(s)$ and closed loop transfer function, $G_{CL}(s)$ are required to be derived and have the bode diagram analysed respectively. $G_{OL}(s)$ for the control system in Figure A.1 can be derived as (A-1) below:

$$G_{OL}(s) = G_c(s) \cdot G_p(s) \tag{A-1}$$

While closed loop transfer function $G_{CL}(s)$ is shown below (A-2):

$$G_{CL}(s) = \frac{G_{OL}(s)}{1 + G_{OL}(s)} \tag{A-2}$$

Figure A.2 is a generic bode diagram of $G_{OL}(s)$ for the magnitude and phase angle as a function of frequency. The frequency at which the open loop gain at unity (0dB) is defined as crossover frequency, f_c. It is well documented that f_c shall be chosen at one to two times smaller than switching frequency, f_{sw} due to interference from switching frequency [39].

At f_c, phase delay introduced by the $G_{OL}(s)$ has to be lesser than 180° in order for the closed loop feedback system to be stable. Thus at f_c the phase angle θ_{OL} measured with respect of -180° is defined as phase margin (PM). For satisfactory dynamic response without oscillations, PM should be greater than 45°, preferably close to 60° [27].

Besides PM, another measure of proximity to instability is the gain margin (GM). It is defined as the scale of gain needed for an unity (0dB) open loop gain at frequency where phase angle is -180º (modulus 360º). For a stable and satisfactory dynamic response, GM should be more than 3dB. Thus a combination of proper GM and PM results in reasonable compensation between bandwidth and stability [54]. It is important to note that by increasing open loop gain, it will only change the open loop magnitude plot while the open loop phase angle plot remains the same. In this way, one can adjust the system to the desired f_c, PM and GM.
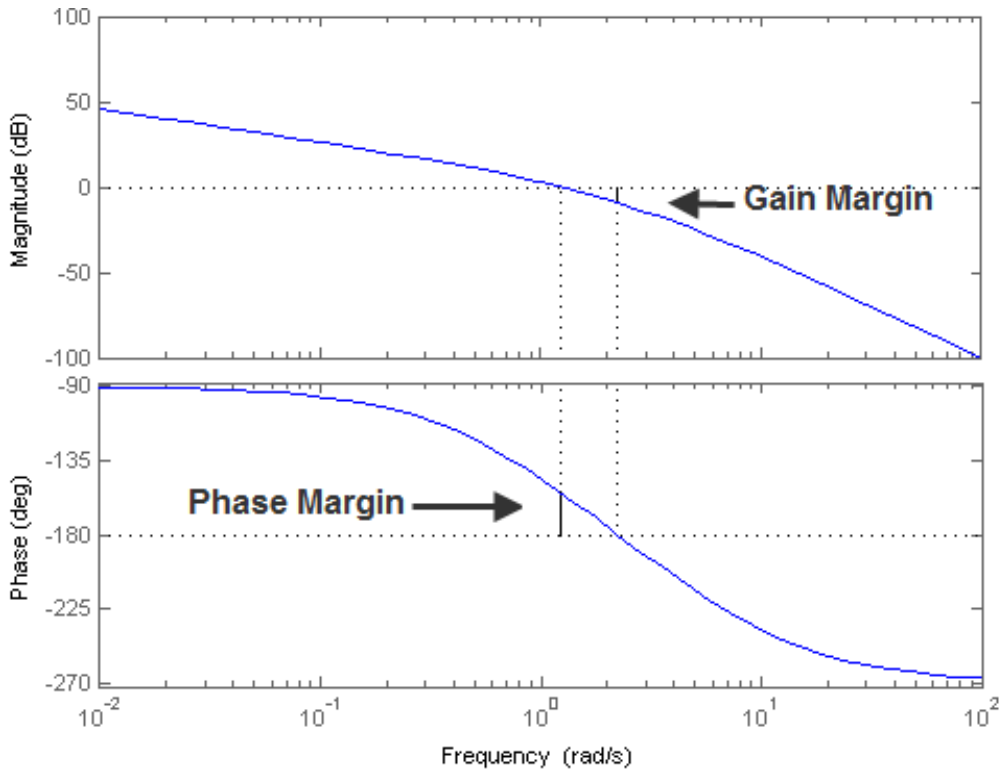

Figure A.2: Generic bode diagram for open loop transfer function [54]

Magnitude of $G_{CL}(s)$ is plotted as in Figure A.3 where the bandwidth (BW) is defined as the frequency at which the gain drops to -3dB, in many practical system bandwidth is similar with f_c. For a fast transient response by the control system, design of closed loop BW should be high which means the design of open loop f_c should be high too.
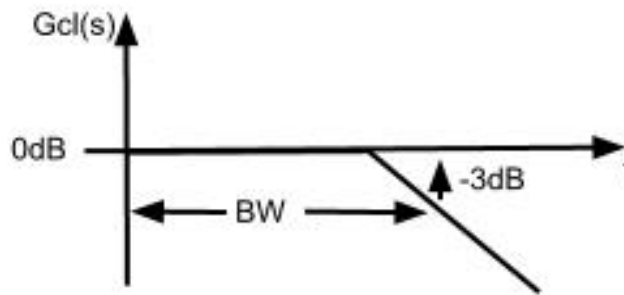

Figure A.3: Generic closed loop magnitude bode plot [27]

APPENDIX B: PI CONTROLLER TUNING TABLE

According to book PID Controllers: Theory, Design, and Tuning by KarlJ. Astrom Tore Hagglund [36], a systematic design procedure for modulus and symmetrical optimization can be done by simplification of system transfer function into desired form. Some of the relevant forms are presented here for reference:

$$G_1(s) = \frac{K}{1 + sT}$$

$$G_2(s) = \frac{K}{(1 + sT_1)(1 + sT_2)} \qquad , T_1 > T_2$$

$$G_3(s) = \frac{K}{(1 + sT_1)(1 + sT_2)(1 + sT_3)} \qquad , T_1 > T_2 > T_3$$

$$G_4(s) = \frac{K}{s(1 + sT)}$$

$$G_5(s) = \frac{K}{s(1 + sT_1)(1 + sT_2)} \qquad , T_1 > T_2$$

Table B.1: Tuning rules for modulus optimum and symmetrical optimum [36]

Transfer function	Controller	Optimization	K_p	T_i	T_d
$G_1(s)$	I	MO	$\dfrac{0.5}{K}$	T	-
$G_2(s)$	P	MO	$\dfrac{T_1}{2KT_2}$	-	-
$G_2(s)$	PI	MO	$\dfrac{T_1}{2KT_2}$	T_1	-
$G_2(s)$	PI	SO	$\dfrac{T_1}{2KT_2}$	$4T_2$	-
$G_3(s)$	PD	MO	$\dfrac{T_1}{2KT_3}$	-	T_2
$G_3(s)$	PID	MO	$\dfrac{T_1 + T_2}{2KT_3}$	$T_1 + T_2$	$\dfrac{T_1 T_2}{T_1 + T_2}$
$G_3(s)$	PID	SO	$\dfrac{T_1(T_2 + 4T_3)}{8KT_3^2}$	$T_2 + 4T_3$	$\dfrac{4T_2 T_3}{T_2 + 4T_3}$

$G_4(s)$	P	MO	$\dfrac{1}{2KT}$	-	-
$G_4(s)$	PI	SO	$\dfrac{1}{2KT}$	$4T$	-
$G_5(s)$	PD	MO	$\dfrac{1}{2KT_2}$	-	T_1
$G_5(s)$	PD	SO	$\dfrac{T_1}{8KT_2{}^2}$	-	$4T_2$
$G_5(s)$	PID	SO	$\dfrac{T_1+4T_2}{8KT_2{}^2}$	T_1+4T_2	$\dfrac{4T_1T_2}{T_1+4T_2}$

APPENDIX C: PRINCIPAL DRAWINGS OF SIMULATION MODELS

Due to right of ownership by Wärtsilä, principal drawings of simulation model in Appendix C is limited from publishing.